

This article was downloaded by: [Monash University Library]

On: 04 December 2014, At: 21:42

Publisher: Taylor & Francis

Informa Ltd Registered in England and Wales Registered Number: 1072954 Registered office: Mortimer House, 37-41 Mortimer Street, London W1T 3JH, UK



Australian Journal of Earth Sciences: An International Geoscience Journal of the Geological Society of Australia

Publication details, including instructions for authors and subscription information:

<http://www.tandfonline.com/loi/taje20>

Geochemistry and geology of spatially and temporally associated calc-alkaline (I-type) and K-rich (A-type) magmatism in a Carboniferous continental arc setting, Pataz gold-mining district, northern Peru

W. K. Witt^a, S. G. Hagemann^a & C. Villanes^b

^a Centre for Exploration Targeting, University of Western Australia, Stirling Highway, Crawley, WA 6009, Australia

^b Compania Minera de Poderosa S.A., Avenida Primavrea 834, Chacarilla del Estanque, Santiago de Surco, 33, Lima, Peru

Published online: 12 Jul 2013.

To cite this article: W. K. Witt, S. G. Hagemann & C. Villanes (2014) Geochemistry and geology of spatially and temporally associated calc-alkaline (I-type) and K-rich (A-type) magmatism in a Carboniferous continental arc setting, Pataz gold-mining district, northern Peru, Australian Journal of Earth Sciences: An International Geoscience Journal of the Geological Society of Australia, 61:1, 17-42, DOI: [10.1080/08120099.2013.797025](https://doi.org/10.1080/08120099.2013.797025)

To link to this article: <http://dx.doi.org/10.1080/08120099.2013.797025>

PLEASE SCROLL DOWN FOR ARTICLE

Taylor & Francis makes every effort to ensure the accuracy of all the information (the "Content") contained in the publications on our platform. However, Taylor & Francis, our agents, and our licensors make no representations or warranties whatsoever as to the accuracy, completeness, or suitability for any purpose of the Content. Any opinions and views expressed in this publication are the opinions and views of the authors, and are not the views of or endorsed by Taylor & Francis. The accuracy of the Content should not be relied upon and should be independently verified with primary sources of information. Taylor and Francis shall not be liable for any losses, actions, claims, proceedings, demands, costs, expenses, damages, and other liabilities whatsoever or howsoever caused arising directly or indirectly in connection with, in relation to or arising out of the use of the Content.

This article may be used for research, teaching, and private study purposes. Any substantial or systematic reproduction, redistribution, reselling, loan, sub-licensing, systematic supply, or distribution in any form to anyone is expressly forbidden. Terms & Conditions of access and use can be found at <http://www.tandfonline.com/page/terms-and-conditions>



Geochemistry and geology of spatially and temporally associated calc-alkaline (I-type) and K-rich (A-type) magmatism in a Carboniferous continental arc setting, Pataz gold-mining district, northern Peru

W. K. WITT^{1*}, S. G. HAGEMANN¹ and C. VILLANES²

¹Centre for Exploration Targeting, University of Western Australia, Stirling Highway, Crawley, WA 6009, Australia

²Compania Minera de Poderosa S.A., Avenida Primavrea 834, Chacarilla del Estanque, Santiago de Surco, 33, Lima, Peru

The Pataz–Parcoy gold-mining area, in the Eastern Andean Cordillera of northern Peru, is located on the western margin of the Amazonia craton, in a transtensional jog on the Cordillera Blanca Fault. Episodic subduction, accretion and rifting have taken place in the Eastern Andean Cordillera since the Mesoproterozoic. In the Pataz district, the Cambrian–Ordovician Vijus and Atahualpa formations comprise dacitic and rhyodacitic volcanoclastic rocks that formed by fractionation and/or crustal assimilation of a regionally more abundant andesitic parent melt. Mississippian magmatism began with enriched tholeiitic magmas that lack a Ti anomaly and formed by melting undepleted metasomatised asthenosphere. These magmas assimilated variable amounts of continental crust and were emplaced as Vista Florida Group volcanoclastic rocks, and dioritic plutons of the Pataz batholith. Ponding of these mantle-derived magmas in andesitic lower crust caused partial melting, which generated the volumetrically dominant, granodioritic component of the calc-alkaline (I-type) Pataz batholith. Within a few million years but following rifting, and uplift of the Pataz batholith, relatively K-rich (A-type) magmas formed by melting of a mid-crustal tonalitic source, and were emplaced in the upper crust as the latitic to rhyolitic Lavasen Volcanics and Esperanza subvolcanic complex. Anatexis in the mid crust was promoted by a second batch of magma derived from the undepleted metasomatised asthenosphere, evidence of which is preserved as mafic components of the Esperanza subvolcanic complex and post-Esperanza dolerite dykes. A K-rich magma chamber, the source of the Lavasen Volcanics and the Esperanza subvolcanic complex, is proposed as a possible source of the ore fluid, which deposited gold in veins hosted by the Pataz batholith.

KEY WORDS: geochemistry, geology, calc-alkaline, I-type, K-rich, A-type, magmatism, Carboniferous, Pataz, gold, Eastern Andean Cordillera Peru.

INTRODUCTION

The Pataz–Parcoy gold field is located near the western boundary of the Eastern Andean Cordillera, on the western margin of the Archean to Paleoproterozoic Amazonia craton (Figure 1). The Pataz district, in the northern part of the Pataz–Parcoy gold-mining area, is a rift and graben terrane resulting from Carboniferous and Cenozoic extensional tectonic events superimposed on a continental margin subduction zone (Witt *et al.* 2013a). Two major igneous episodes occurred during the Mississippian (early Carboniferous), and relevant geochronological data for these episodes are summarised in Table 1. These intrusive and extrusive rocks were emplaced into or onto latest Neoproterozoic to Ordovician basement and volcano-sedimentary units of the Eastern Andean Cordillera. The first Mississippian magmatic episode

resulted in emplacement of the Pataz batholith, an elongate, NNW-trending body of granodiorite and diorite that hosts the majority of the auriferous quartz–carbonate–sulfide veins (Haerberlin *et al.* 2004). SHRIMP (Witt *et al.* 2013a) and ID-TIMS (Schaltegger *et al.* 2006) U–Pb in zircon geochronology indicates an age of 338–336 Ma for the emplacement of the Pataz batholith in the Pataz district. A U–Pb in zircon age of 329 Ma (Table 1) from granodiorite in the Parcoy district suggests intrusive activity may have migrated southwards over time. The second Carboniferous igneous event followed shortly after emplacement of the Pataz batholith and resulted in deposition of the Lavasen Volcanics in the Lavasen rift at *ca* 334 Ma (Witt *et al.* 2013b). The Esperanza subvolcanic complex, which gives a SHRIMP zircon age within error of that for the Lavasen Volcanics, was emplaced into the western margin of the rift, adjacent to the Pataz batholith.

*Corresponding author: wittww@inet.net.au

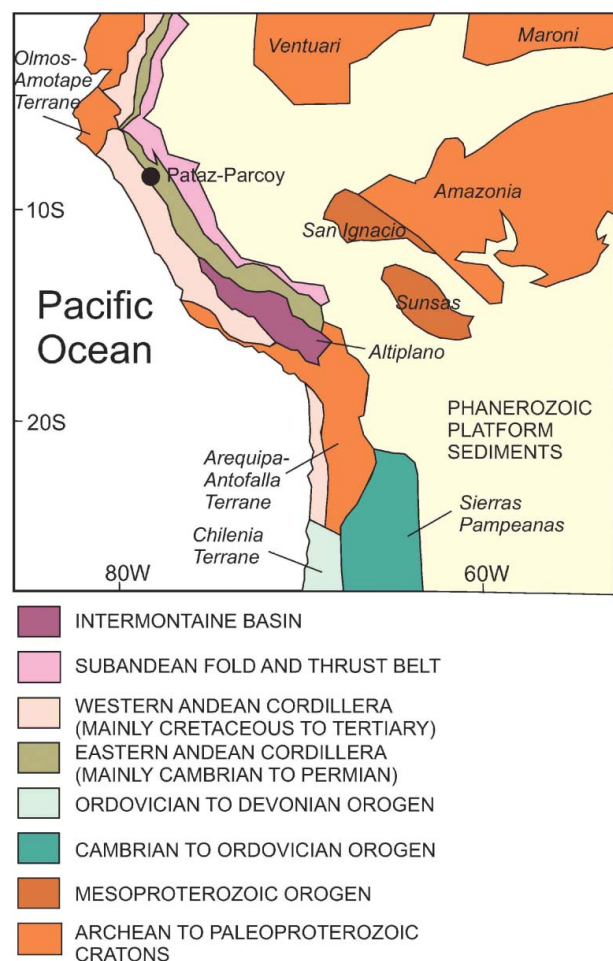


Figure 1 Regional geological setting of the Pataz-Parcoy mining area, based on Miskovic *et al.* (2009).

There are limited published whole-rock geochemical data for the Pataz batholith. Schreiber *et al.* (1990) presented some basic classification diagrams and concluded that the batholith comprised calc-alkaline, I-type granites. Their samples fall in the volcanic arc field on an Rb vs Y+Nb plot (Pearce *et al.* 1984), although Schreiber *et al.* (1990) suggested that, based on structural setting of the intrusions, they should be classified as post-collision granites. Macfarlane *et al.* (1999) reported Pb and Nd isotope data for the Pataz batholith, which they interpreted to show that the batholith-forming magmas had interacted substantially with older continental crust. Miskovic *et al.* (2009) reported whole-rock geochemical data from a regional study of granitic intrusions in the Eastern Andean Cordillera, with samples collected between 6°S and 16°S. Of these, several samples came from the Pataz batholith, but none were reported from the Pataz district. Carboniferous granites of the Eastern Andean Cordillera (such as the Pataz batholith) were classified as Cordilleran-type, continental-arc-related intrusions by Miskovic *et al.* (2009). In this contribution, we present whole-rock geochemical data for three groups of igneous rocks in the Pataz district (the northern half of the Pataz-Parcoy gold-mining area). The earliest group comprises early Paleozoic felsic to intermediate volcanic rocks of the Vijus and Atahualpa

formations. The other two groups are both Mississippian in age and comprise the calc-alkaline Pataz batholith and the slightly younger, K-rich volcanic and subvolcanic rocks (the Lavasen Volcanics and Esperanza subvolcanic complex, respectively). We discuss the implications of these data for the tectonic evolution of the Pataz district and for the origin of the batholith-hosted gold mineralisation.

REGIONAL SETTING

The Pataz-Parcoy gold-mining area is located in a transtensional jog on the regional Cordillera Blanca Fault (Petford & Atherton 1992; Witt *et al.* 2013a), which separates the Eastern Andean Cordillera from the Western Andean Cordillera (Megard 1984). The transtensional jog coincides with a north-striking section of the mainly NNW-striking Cordillera Blanca Fault, and the Pataz district is dominated structurally by NW- to NNW-striking faults and NE- to ENE-striking lineaments (Figure 2). The main gold-mining areas at Pataz are located in Mississippian intrusions and Neoproterozoic basement, at the western margin of the Eastern Andean Cordillera. Targeting methods for gold in these areas are described in a companion paper (Witt *et al.* 2013b).

Although the Western Andean Cordillera is dominated by the effects of the Cenozoic Andean orogeny, earlier orogenic activity was focused along the Eastern Andean Cordillera, which was the leading continental margin of western Amazonia for at least 900 Ma (Miskovic & Schaltegger 2009). Intrusive rocks of the Eastern Andean Cordillera are predominantly the products of major pulses of magmatic activity in the Carboniferous to early Permian (340–285 Ma continental arc magmas) and again in the middle Permian to Early Jurassic (275–190 Ma extension-related granites), with volumetrically subordinate plutons related to modern Andean subduction (Miskovic *et al.* 2009).

GEOLOGY OF THE PATAZ DISTRICT WITH EMPHASIS ON THE IGNEOUS ROCKS

The geology and structural evolution of the Pataz district was described by Witt *et al.* (2013a), and the principle igneous units of interest are summarised in Table 2. The Mississippian Pataz batholith and its early Paleozoic country rocks are exposed in a central NNW-trending horst (Figure 2). The Pataz batholith was emplaced at *ca* 338–336 Ma (Table 1; Schaltegger *et al.* 2006), during the Gondwanide orogeny. Emplacement of the batholith was facilitated by intermittent extension in the Pataz-Parcoy transtensional jog during NE–SW Gondwanide shortening, which resulted in dextral strike-slip movement on the Cordillera Blanca Fault. Differential uplift occurred shortly after emplacement of the batholith. At this time, the batholith-hosted auriferous veins formed, and the Lavasen Volcanics were deposited in a graben (the Lavasen graben) to the east of the central horst (Witt *et al.* 2013a; Figure 2). An allochthonous sedimentary sequence, deposited in the Western Andean Cordillera, was thrust over the Eastern Andean Cordillera during the Upper Cretaceous Peruvian phase of the Andean orogeny (Megard 1984). In the Pataz

Table 1 Summary of Paleozoic geochronological data for emplacement of Paleozoic igneous units and related events, Pataz-Parcoy gold-mining area.

| Unit | Location | Lithology | Method | Age | Source |
|--|------------------------------|--------------------------------------|--|--|---------------------------------------|
| Alkaline intrusion | SE Pataz | Quartz monzonite | U-Pb in zircon (LA_ICP_MS) | 301 ± 5.2 Ma ca 312 Ma | Miskovic <i>et al.</i> (2009) |
| Gondwanide orogeny | | | | | Schaltegger <i>et al.</i> (2006) |
| Mineralisation | La Lima, Pataz district | Granodiorite | ⁴⁰ Ar- ³⁹ Ar; white mica | 312.1 ± 0.8 Ma | Haerberlin <i>et al.</i> (2004) |
| Mineralisation | El Tingo, Pataz district | Granodiorite | ⁴⁰ Ar- ³⁹ Ar; fuchsite | 313.5 ± 1.4 Ma | Haerberlin <i>et al.</i> (2004) |
| Mineralisation | Consuelo, Pataz district | Granodiorite | ⁴⁰ Ar- ³⁹ Ar; white mica | 314.1 ± 1.2 Ma | Haerberlin <i>et al.</i> (2004) |
| Pataz batholith | Paraiso, Pataz district | Aplite | ⁴⁰ Ar- ³⁹ Ar; muscovite | 322.1 ± 2.8 Ma | Haerberlin <i>et al.</i> (2004) |
| Pataz batholith | Paraiso, Pataz district | Aplite | ⁴⁰ Ar- ³⁹ Ar; biotite | 325.4 ± 1.4 Ma | Haerberlin <i>et al.</i> (2004) |
| Pataz batholith | Papagayo, Pataz district | Granodiorite | ⁴⁰ Ar- ³⁹ Ar; biotite | 328.1 ± 1.2 Ma | Haerberlin <i>et al.</i> (2004) |
| Pataz batholith | Parcoy district | Granodiorite | U-Pb in zircon | 329 Ma | Macfarlane <i>et al.</i> (1999) |
| Pataz batholith | Paraiso, Pataz district | Monzogranite | ⁴⁰ Ar- ³⁹ Ar; biotite | 329.2 ± 1.4 Ma | Haerberlin <i>et al.</i> (2004) |
| Mineralisation | Parcoy district | Quartz-arsenopyrite-molybdenite vein | Re-Os in molybdenite | 331.9 ± 1.7 Ma | Szappanosné-Vágó <i>et al.</i> (2010) |
| Alkaline intrusion | Central Pataz | Monzogabbro | U-Pb in zircon (LA_ICP_MS) | 333.2 ± 7.7 Ma | Miskovic <i>et al.</i> (2009) |
| Esperanza subvolcanic complex | Paraiso, Pataz district | Latite porphyry | U-Pb in zircon (SHRIMP) | 333.7 ± 2.4 Ma | Witt <i>et al.</i> (2013a) |
| Lavasen Volcanics | Misquichilca, Pataz district | Resedimented pumice-rich breccia | U-Pb in zircon (SHRIMP) | 334.3 ± 1.8 Ma | Witt <i>et al.</i> (2013a) |
| Pataz batholith | Patataz district | Albitite dyke | U-Pb in zircon (ID-TIMS) | 336.4 ± 0.6 Ma | Schaltegger <i>et al.</i> (2006) |
| Pataz batholith | Paraiso, Patataz district | Metamorphosed | U-Pb in zircon (SHRIMP) | Minimum age of 338 ± 3 Ma | Witt <i>et al.</i> (2013a) |
| Atahualpa Formation, top of Eastern Andean Cordillera sequence | Between Cedro and Patataz | volcaniclastic sediment | U-Pb in zircon (SHRIMP) | 466.8 ± 8.1 Ma | Witt <i>et al.</i> (2013a) |
| Pampean orogeny | | | | | Chew <i>et al.</i> (2007) |
| Maranon Complex | | Basement schists | | ca 460 Ma Latest Neoproterozoic to early Cambrian | Haerberlin <i>et al.</i> (2004) |

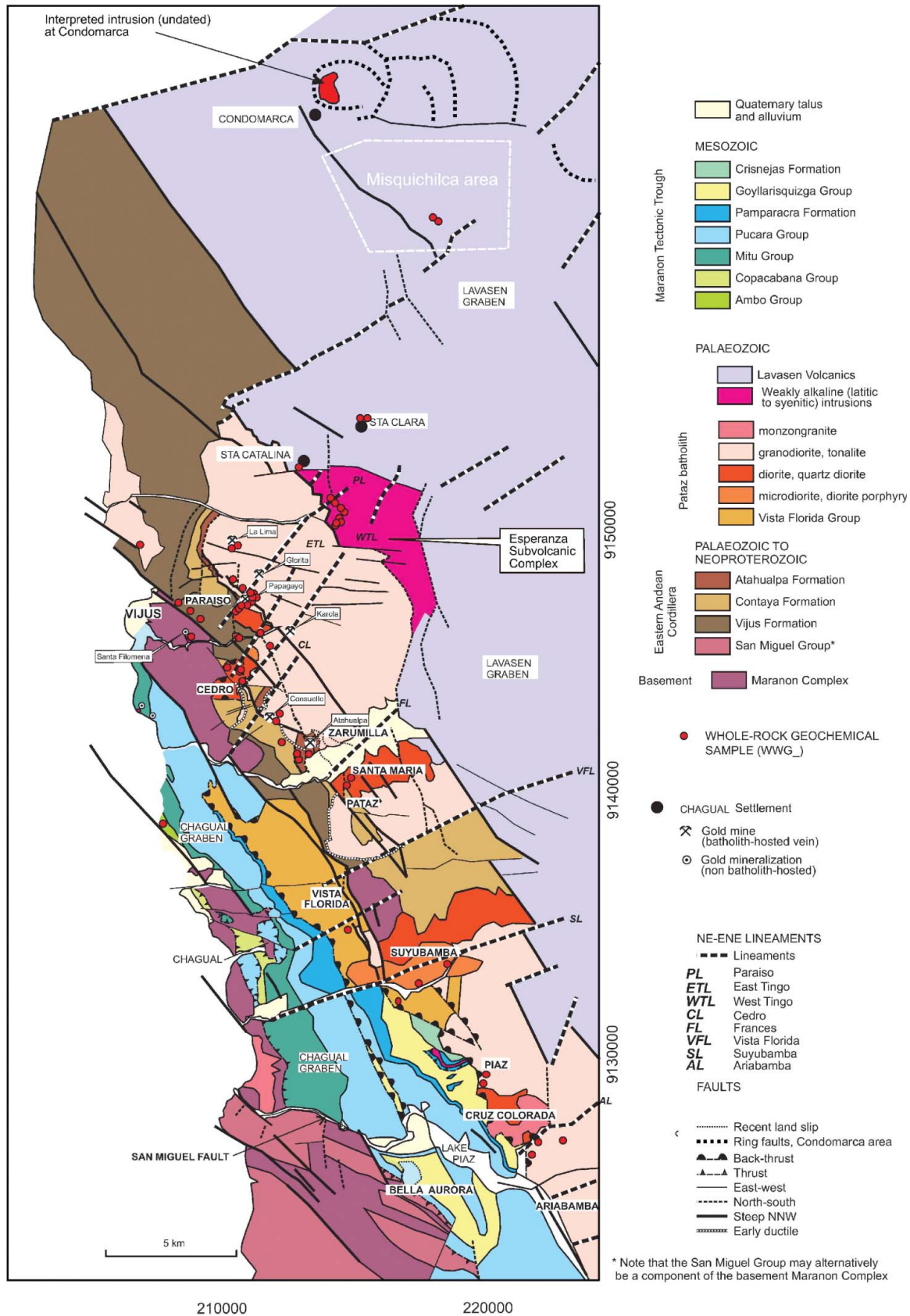


Figure 2 Geological map of the Pataz district showing location of gold mines and other localities discussed in the text. Also shown are the locations of whole-rock geochemical samples reported in this publication. The blank area to the west of the geological map lies to the west of the Maranon River and has not been mapped at 1:25 000. Except for the Misquichilca area (outlined), the area north of Santa Catalina only been mapped by photo-interpretation and a single traverse between Santa Catalina and Misquichilca.

Table 2 Summary of petrographic features of igneous rocks in the Pataz district.

| Unit | Mineralogy | Textural features | Magma type | Age |
|---|---|---|--|---------------------------------------|
| Esperanza subvolcanic complex dolerite | Dolerite | Subophitic to weakly porphyritic | Enriched subalkaline to slightly alkaline tholeiitic | Mississippian (post-334 Ma) |
| Lavasen volcanic rocks | Latite to rhyolite: albite and K-feldspar, minor quartz, phenocrysts | Volcanic flow and volcanoclastic textures | Ferroan, calc-alkalic A-type | Mississippian (334 Ma) |
| Esperanza subvolcanic complex latites | (Quartz-) latite porphyry: albite and K-feldspar ± quartz phenocrysts; quartz partially resorbed | Porphyritic; flow textures, spherulitic | Ferroan, calc-alkalic A-type | Mississippian (334 Ma) |
| Pataz batholith high-SiO ₂ suite | Granodiorite, subordinate tonalite, monzogranite: biotite (± hornblende) | Massive to seriate to porphyritic | Magnesian to ferroan, calcic to calc-alkalic I-type | Mississippian (336–338 Ma) |
| Pataz batholith low-SiO ₂ suite | Diorite, quartz diorite, tonalite and volcanic equivalents: hornblende (± clinopyroxene, biotite) | Massive to cumulate-textured | Magnesian, calcic to calc-alkalic I-type | Mississippian (pre- <i>ca</i> 336 Ma) |
| Estrella monzonite porphyry | Monzonite porphyry: K-feldspar phenocrysts | Porphyritic | Shoshonitic A-type | ?Silurian (466 ± 5 Ma) |
| Vijus and Atahualpa Groups | Andesitic to dacitic | Volcanoclastic | Calc-alkaline | Cambrian–Ordovician |

district, this allochthonous sequence has mostly been removed by erosion, but is locally preserved in the Chagual graben, to the west of the central horst. The Chagual graben formed during a Cenozoic, extensional phase of the Andean orogeny.

The country rocks of the Pataz batholith belong to the Eastern Andean Cordillera and comprise late Neoproterozoic to early Cambrian basement (the Marañon Complex) and overlying Cambrian–Ordovician volcano-sedimentary units (from oldest to youngest: the Vijus Formation, the Contaya Formation and the Atahualpa Formation; Figure 2 and Witt *et al.* 2013a). Whereas the Contaya Formation is predominantly sedimentary, the Vijus and Atahualpa formations are felsic to intermediate volcanoclastic rocks that contain millimetre-scale quartz- and biotite-rich aggregates, possibly devitrified vitric clasts, and crystal fragments of plagioclase, quartz and biotite. Typical outcrops of the Vijus Formation preserve igneous textures but are strongly fractured and contain variable amounts of hydrothermal sericite, chlorite, clay minerals and iron oxides. The Atahualpa Formation has a stronger ductile deformation fabric but lithic or devitrified vitric clasts and mineral clasts are easily recognised within the foliated rock. The Atahualpa Formation was deposited shortly after 466 Ma (Table 1).

Field and petrographic features of the Pataz batholith are described by Schreiber *et al.* (1990), Macfarlane *et al.* (1999), Haerberlin *et al.* (2004) and Witt *et al.* (2013a). The main component of the batholith is massive, medium- to coarse-grained, equigranular; biotite (± hornblende) granodiorite and less common tonalite. Sharp contacts between granodiorite and tonalite have not been observed. There is minor textural variation within the granodiorite but internal contacts are rare, and gradational. The granodiorite locally contains hornfelsed xenoliths of the Contaya Formation. The other major component of the batholith is dioritic, ranging from

medium- to coarse-grained diorite and quartz diorite to diorite porphyry and microdiorite. Hornblende is typically dominant over biotite in these rocks, and relict cores of clinopyroxene have been observed locally. The dioritic component has been emplaced in and adjacent to NE–ENE lineaments that cut the batholith (Figure 2). Medium- to coarse-grained biotite monzogranite and dykes of aplite and pegmatite are minor components of the batholith. Sharp xenolithic contacts generally indicate that the dioritic component has been intruded by the dominant granodiorite component, but magma-mingling structures have also been observed, indicating that the two magmas were partly contemporaneous (Witt *et al.* 2013a).

The newly recognised Vista Florida Formation (Witt *et al.* 2013a) comprises mafic to intermediate volcanoclastic sandstone, siltstone and breccia, and minor lava flows. This unit outcrops to the west of the Pataz batholith, between the Cedro and Suyubamba lineaments (Figure 2) and is separated from the batholith by the Vijus fault. The western contact is a back-thrust, which has emplaced the Vista Florida Formation over the younger allochthonous sedimentary rocks (Witt *et al.* 2013a). The volcanoclastic rocks are host to a minor component of microdiorite and diorite porphyry, which are petrographically indistinguishable from equivalent rocks that form parts of the batholith.

The Lavasen Volcanics comprise plagioclase- and K-feldspar-phyric latitic to rhyolitic pyroclastic rocks, resedimented pyroclastic rocks and volcanogenic sedimentary rocks. Over 3000 m of volcanoclastic deposits accumulated in the Misquichilca area (Figure 2) has shown the volcanic sequence in that area to be gently folded and subdivided by NNW-striking faults into a series of second order grabens and horsts (Witt *et al.* 2013a). Recent geochronological data (Table 1) have shown that the Lavasen Volcanics are Mississippian in age (*ca* 334 Ma),

contrary to previous estimates of Cenozoic deposition (Reyes & Wilson 1964; Wilson & Reyes 1997).

The Esperanza subvolcanic complex was emplaced along the western margin of the Lavasen graben and has a faulted contact with the Patáz batholith (Figure 2). It is a high-level, bimodal complex, comprising latite porphyry and quartz latite porphyry, and a subordinate component of dolerite (Witt *et al.* 2013a). Latitic rocks contain up to 15% but mostly <5% phenocrysts of plagioclase and K-feldspar. Quartz phenocrysts in the quartz latite porphyry are partially resorbed. Flow banding and spherulitic textures are well developed in the latite and quartz latite porphyries, and the complex is interpreted as a possible flow dome complex. Weak potassic and argillic hydrothermal alteration are widespread. Cognate clots of coarse-grained plagioclase with pyroxene, Fe-rich dark green amphibole and green (Fe^{3+} -rich) biotite suggest derivation of the latitic rocks from a subjacent magma chamber. Dolerite dykes intrude the latitic porphyries. Dark green amphibole and pleochroic relict clinopyroxene in the dolerite indicate Fe-rich mineral compositions, confirmed by EDS analysis of amphiboles using a SEM at the Centre for Microscopy, Characterisation and Analysis, University of Western Australia ($\text{Fe} + \text{Mn} + \text{Ti}/\text{Fe} + \text{Ti} + \text{Mn} + \text{Mg} = 0.5$ to 0.7 ; Witt *et al.* 2013a). Vari-textured dolerite contains discontinuous, internalised veinlets of plagioclase–magnetite interpreted as late-stage mesostasis. The increasingly calcic composition of plagioclase from early formed phenocrysts (albite) through groundmass (andesine–labradorite) to late-stage plagioclase (bytownite)–magnetite veinlets (Witt *et al.* 2013a) suggests enrichment of a volatile-rich phase during crystallisation of the dolerite magma (cf. Panjasawong *et al.* 1995).

WHOLE-ROCK GEOCHEMISTRY OF IGNEOUS ROCKS IN THE PATAZ DISTRICT

Introduction

Thirty-seven samples were submitted for whole-rock geochemical analysis in two batches. Although most samples came from the Patáz batholith, one sedimentary rock sample from the Contaya Formation was analysed to assess the role of local country rock assimilation on the chemistry of the batholith magmas. A full list of samples with rock type and location, and analytical methods, accuracy and precision, are described in the Supplementary Papers.

Every attempt was made to collect samples with minimum hydrothermal alteration. However, the effects of widespread but mostly low-intensity silicification and argillic alteration of Lavasen Volcanic samples are clearly reflected in the whole-rock geochemical data where analyses for SiO_2 extend beyond the maximum expected for unaltered acid igneous rocks (~ 76 wt%; Cox *et al.* 1980) to as much as 82.7 wt% SiO_2 (Figure 3). Some low- SiO_2 batholith surface outcrop samples display weak to moderate chloritisation and calcite veins (district-wide propylitic alteration), and this is reflected in scattered Na_2O (Figure 3a) and Sr values. Schreiber *et al.* (1990) described intense and extensive alteration of plagioclase to sericite in most samples from the Patáz

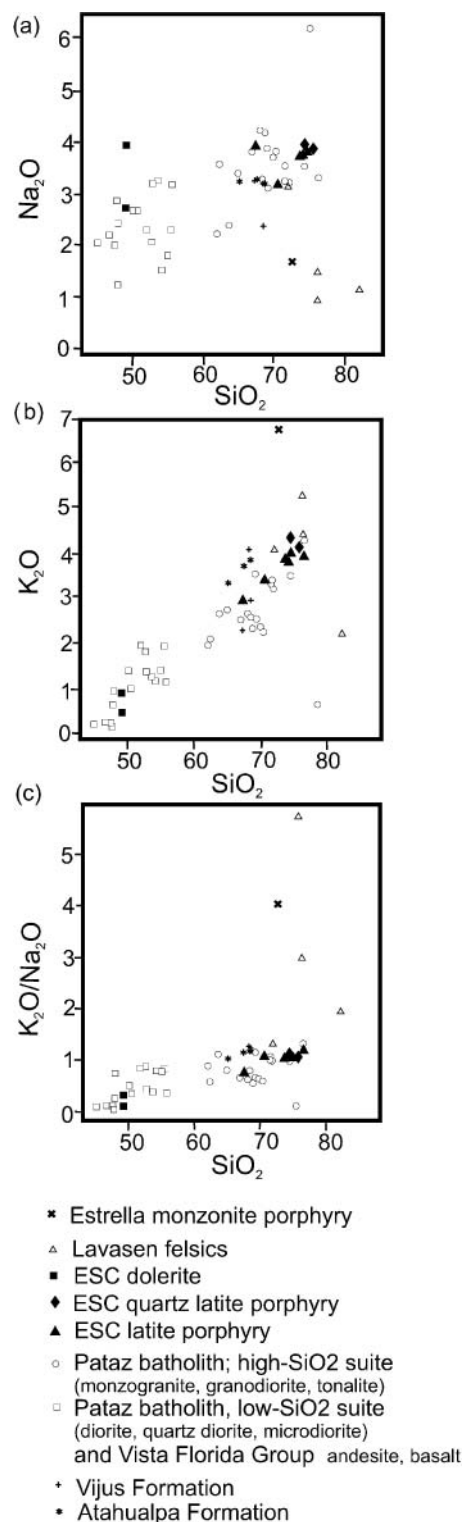


Figure 3 Geochemical plots used to monitor hydrothermal alteration in whole-rock geochemical samples: (a) Na_2O vs SiO_2 , (b) K_2O vs SiO_2 and (c) $\text{K}_2\text{O}/\text{Na}_2\text{O}$ vs SiO_2 . ESC, Esperanza subvolcanic complex.

batholith, and attributed the sericitisation to deuteric alteration by K-rich residual magmatic fluids. The petrographic observation is confirmed by this study. However, limited dispersion on a K_2O vs SiO_2 plot (Figure 3b) suggests that sericitic alteration did not have a major

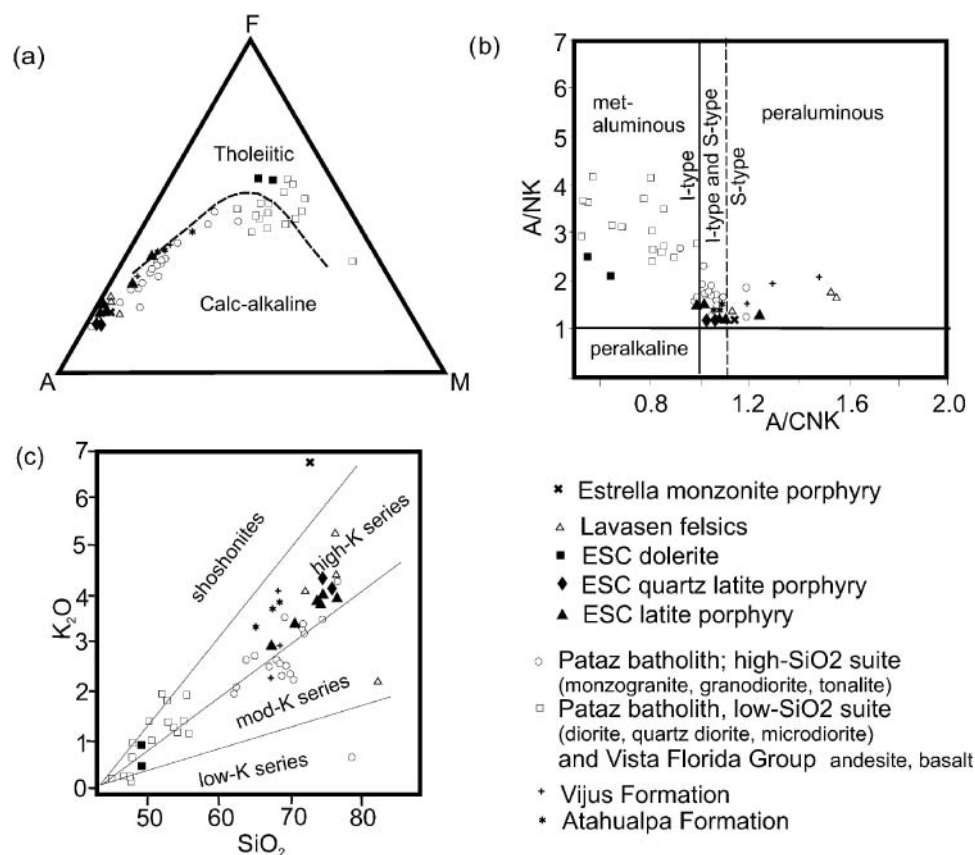


Figure 4 Whole-rock compositions for Pataz district samples: (a) AFM plot, (b) A/NK vs A/CNK plot (after Shand 1943) and (c) K₂O vs SiO₂ (after Pecerillo & Taylor 1979). A = molAl₂O₃, C = molCaO, K = molK₂O, N = molNa₂O. The A/CNK ratio of 1.1 in Figure 4b is the maximum limit for I-type granites according to Chappell & White (1974). ESC, Esperanza subvolcanic complex.

impact on the whole-rock chemistry of most granitoids. Sodium, Sr and, possibly, Ba appear to be the elements most affected by hydrothermal alteration, whereas most other major and trace elements are considered to reflect magmatic compositions. Three samples each of the Vijus and Atahualpa formations form relatively tight clusters on most plots. Their whole-rock chemistry does not appear to have been significantly affected by hydrothermal alteration with the possible exception of alkalis (Na₂O, K₂O), particularly in the Vijus Formation (Figure 3).

Because whole-rock compositions of the Lavasen samples have probably been modified by hydrothermal alteration, relatively immobile elements (particularly Ti, Th, Hf, Zr, Nb, V, Ga) are used to support interpretations based on major elements. The geochemistry of the main igneous groups (Vijus and Atahualpa formations, Pataz batholith and the Vista Florida Group, Lavasen Volcanics and Esperanza subvolcanic complex) is described in turn, from oldest to youngest.

Geochemistry of the Vijus and Atahualpa formations

Samples of the Vijus and Atahualpa formations occupy an SiO₂ range between 65.8 wt% and 70.5 wt% (Supplementary Papers Table A2). They are subalkaline and plot in the calc-alkaline field of an AFM diagram (Figure 4a).

The A/NK vs A/CNK plot (after Shand 1943) shows the Atahualpa samples to be mildly peraluminous whereas the Vijus samples are strongly peraluminous (Figure 4b), possibly reflecting hydrothermal leaching of Ca and alkalis and the formation of secondary sericite, chlorite and clay minerals during metamorphism or hydrothermal alteration. Both groups belong to the high-K calc-alkaline series, according to the K₂O vs SiO₂ plot (Figure 4c, after Pecerillo & Taylor 1979), although the Vijus Formation data are scattered, again perhaps reflecting metamorphism or hydrothermal alteration. As shown in Figure 5a, both groups plot within the rhyodacite/dacite field on an immobile element-based plot developed by Winchester & Floyd (1977), but the Atahualpa Formation plots near the andesite boundary whereas the Vijus Formation plots closer to the rhyolite field.

Discriminative plots developed by Frost *et al.* (2001), classify the Vijus and Atahualpa formations as ferroan (Figure 6a). Most Atahualpa samples plot near the boundary between the calc-alkalic and alkali-calcic associations but the Vijus samples are highly dispersed, again possibly reflecting mobility of alkalis during metamorphism or hydrothermal alteration (Figure 6b). The Vijus and Atahualpa samples are tightly clustered on plots incorporating the immobile elements V, Th and Zr, which effectively distinguish the two groups (Figure 5c).

The Vijus and Atahualpa formations display mildly concave upward REE curves (Figure 7a) with steep light

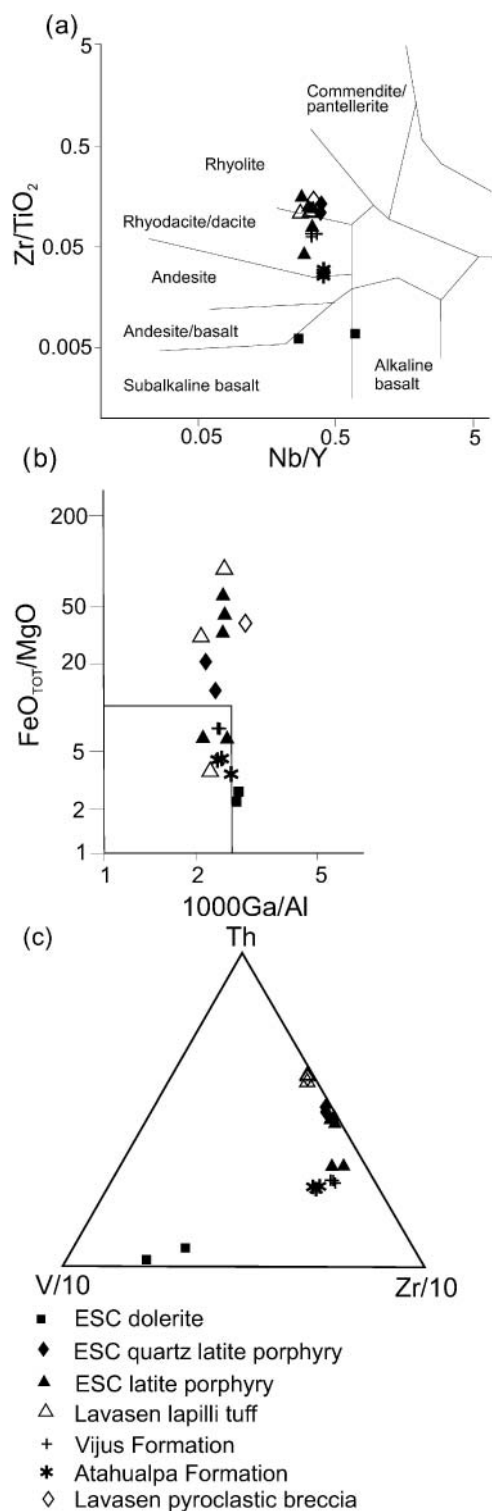


Figure 5 Discriminatory diagrams showing composition of Lavasen Volcanic and Esperanza subvolcanic complex whole-rock samples; Vijus and Atahualpa formation samples are also shown for comparison: (a) Zr/TiO_2 vs Nb/Y (after Winchester & Floyd 1977), (b) FeO_{tot}/MgO vs Ga/Al (after Whalen *et al.* 1987) and (c) Th-V/10-Zr/10. Note that batch 1 samples (mostly Patáz batholith) are not plotted because they were not analysed for Nb, Ga or V. ESC, Esperanza subvolcanic complex.

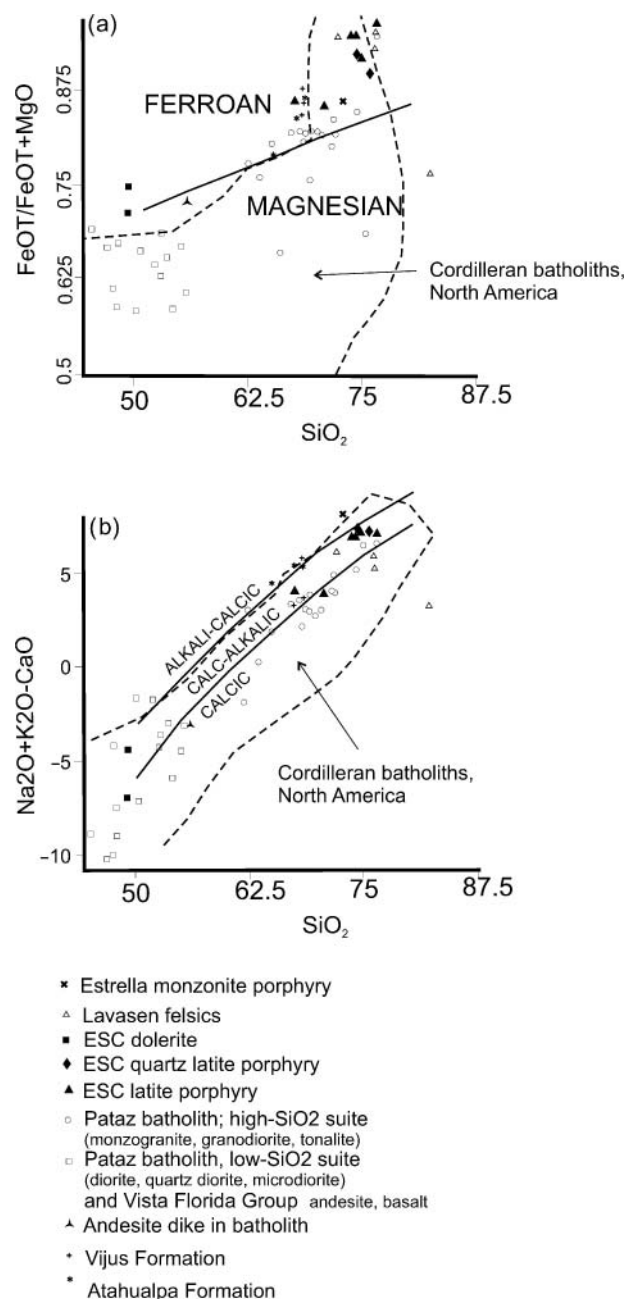


Figure 6 Fe-number and modified MALI diagrams developed by Frost *et al.* (2001) for the geochemical classification of granites, showing data from Patáz. For comparison, the field of 344 Mesozoic Cordilleran batholith samples from North America (after Frost *et al.* 2001) is shown. ESC, Esperanza subvolcanic complex.

rare earth elements (LREE), a moderate negative Eu anomaly and relatively flat heavy rare earth elements (HREE). The $(La/Sm)_N$ ratios range between 2.56 and 3.66 and $(La/Yb)_N$ ratios between 5.25 and 7.61. Compared with the Atahualpa Formation, the Vijus samples have slightly deeper Eu anomalies and lower HREE but the LREE abundances are almost identical. The two groups of samples display very similar NMORB-normalised multi-element spidergrams (Figure 8). The spidergrams show enrichment of incompatible elements (left side of

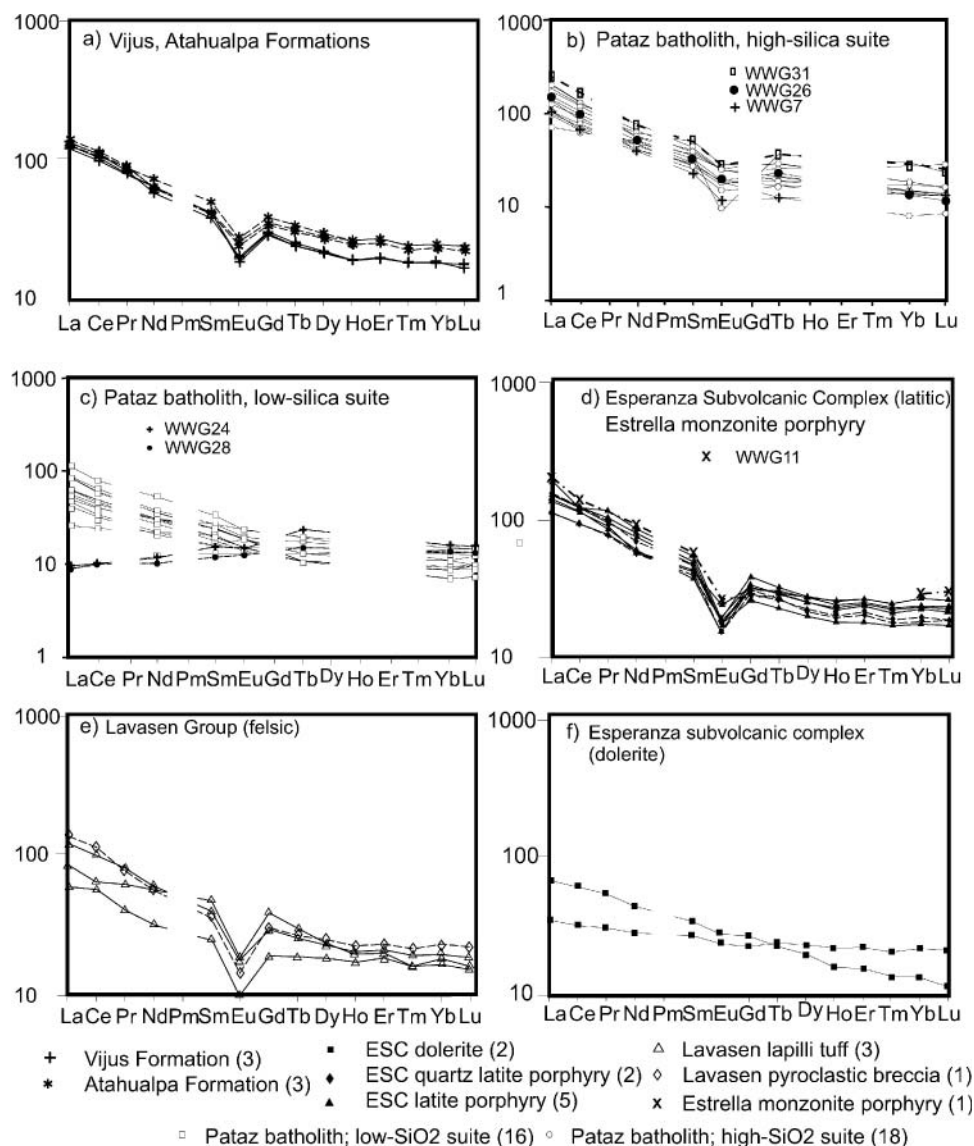


Figure 7 REE plots for Pataz district samples (normalised to chondrite values of Boynton 1984). (a) Vijus and Atahualpa formations, (b) Pataz batholith—high-SiO₂ samples, (c) Pataz batholith and Vista Florida Group—low-SiO₂ samples, (d) Esperanza subvolcanic complex—latitic samples, (e) Lavasen Volcanics and (f) Esperanza subvolcanic complex—dolerite. ESC, Esperanza subvolcanic complex.

the plots), negative Nb, Sr (\pm P) and Ti anomalies, and positive Pb anomalies.

Geochemistry of the Pataz batholith and Vista Florida Group

Collectively, the Pataz batholith and Vista Florida Group samples define an SiO₂ range between 45.0 wt% and 76.4 wt% (Supplementary Papers Table A2). The data plot in the calc-alkaline field on an AFM diagram, although low-SiO₂ samples straddle the calc-alkaline/tholeiite boundary (Figure 4a). Schreiber *et al.* (1990) classified granites of the Pataz batholith as I-type, consistent with the widespread presence of hornblende in diorite and tonalite, and, less consistently, in granodiorite. The I-type classification is also consistent with an A/CNK (Al₂O₃/CaO + Na₂O + K₂O) ratio <1.1 (Chappell

& White 1974, 1992) for the bulk of the analyses (Figure 4b). Most of the data straddle the moderate to high-K calc-alkaline fields in an SiO₂ vs K₂O plot (Figure 4c). On plots developed by Frost *et al.* (2001), low-SiO₂ samples, including the Vista Florida Group, are magnesian, whereas high-SiO₂ samples straddle the magnesian/ferroan boundary (Figure 6a); low-SiO₂ samples are scattered, but the high-SiO₂ samples straddle the boundary between calcic and calc-alkalic associations (Figure 6b). The classification illustrated in Figure 6 shows that the Pataz batholith trends are similar to those of calc-alkaline Cordilleran batholiths such as the Tuolumne Suite and the northern Idaho batholith. These are subduction-related magmas typical of continental margin arcs (Bateman & Chappell 1979; Hyndman 1984).

Harker variation diagrams effectively subdivide the majority of batholith samples into two suites: a

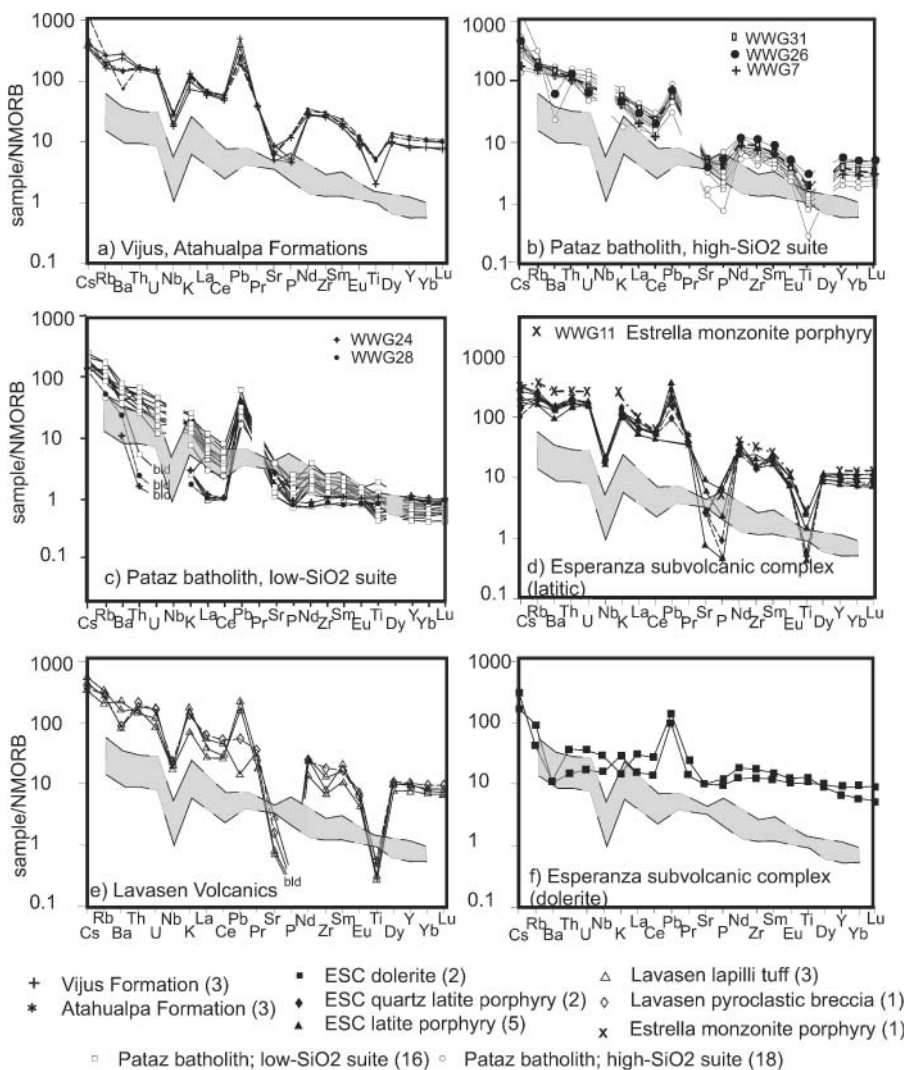


Figure 8 Multi-element diagrams (N-MORB-normalised, after Sun & McDonough 1989) for Patataz district samples. (a) Vijus and Atahualpa formations, (b) Patataz batholith—high-SiO₂ samples, (c) Patataz batholith and Vista Florida Group—low-SiO₂ samples, (d) Esperanza subvolcanic complex—latitic samples, (e) Lavasen Volcanics and (f) Esperanza subvolcanic complex—dolerite. Gaps in lines represent elements for where no analyses are available (Nb, Pr, Dy) or are below the lower level of detection (U). For comparison, the transparent grey envelope encloses four basalts that erupted through thick continental crust in the central Chilean arc (Pearce 1983). ESC, Esperanza subvolcanic complex. Gaps marked bld are values below the analysis detection limit.

low-silica suite and a high-silica suite (Figures 9, 10), separated by a ‘silica gap’ between approximately 55 and 60 wt% SiO₂. The high-silica suite comprises granodiorite and monzogranite, as well as three tonalite samples. The low-silica suite comprises samples of diorite, quartz diorite and diorite porphyry, as well as one tonalite sample. WWG2, a member of the low-silica suite, is a cumulate-textured metapyroxenite and therefore plots away from the main group of low-silica samples on several of the plots in Figures 9 and 10 (see particularly MgO). The two mafic volcanoclastic samples from the Vista Florida Group consistently plot with diorite and microdiorite of the low-silica batholith suite, supporting field evidence for a co-magmatic relationship between the two (Witt *et al.* 2013a). An andesite dyke that intrudes granodiorite of the batholith near the Glorita mine entrance (Figure 2) lies at the high-SiO₂ end of the low-SiO₂ suite and contains relatively high La and P₂O₅, and may belong to a later intrusive event but is here discussed with the low-SiO₂ suite.

Both suites display decreasing MgO, CaO, Fe₂O₃ (total), Co and V, and increasing K₂O, Rb and K₂O/Na₂O ratio with increasing SiO₂, although with some scatter particularly among the low-SiO₂ suite (e.g. Figure 9b).

The high-SiO₂ suite also displays decreasing trends of P₂O₅, TiO₂ and Sc with increasing SiO₂, but these elements produce considerable scatter in the low-SiO₂ suite (e.g. Figure 9g). The elements Ba, Th, Zr and La display contrasting trends between suites, producing an overall increase with SiO₂ in the low-SiO₂ suite and a weak to pronounced decrease with increasing SiO₂ in the high-SiO₂ suite (Figure 10c, e, g, h). Copper produces scatter among the low-SiO₂ suite samples and a decreasing trend in the high-SiO₂ suite (Figure 10a).

REE patterns for the low-silica suite are variably enriched in LREE, with the exception of two samples (WWG24 and WWG28), which are distinctly depleted in LREE (Figure 7c). These two samples are among the most primitive of the low-SiO₂ suite, as indicated by low SiO₂ values and high Mg# (= MgO/MgO + Total Fe as Fe₂O₃). All low-SiO₂ suite samples lack a Eu anomaly. The (La/Yb)_N ratios range between 0.54 and 7.78 and are broadly correlated with SiO₂. REE patterns for the high-silica suite are similar to those of low-silica suite samples but contain higher total REE, lack examples equivalent to the flatter curves generated by the low-SiO₂ suite, and display a weak negative Eu anomaly (Figure 7b). The (La/Yb)_N ratios range between 2.48 and 13.54 with a

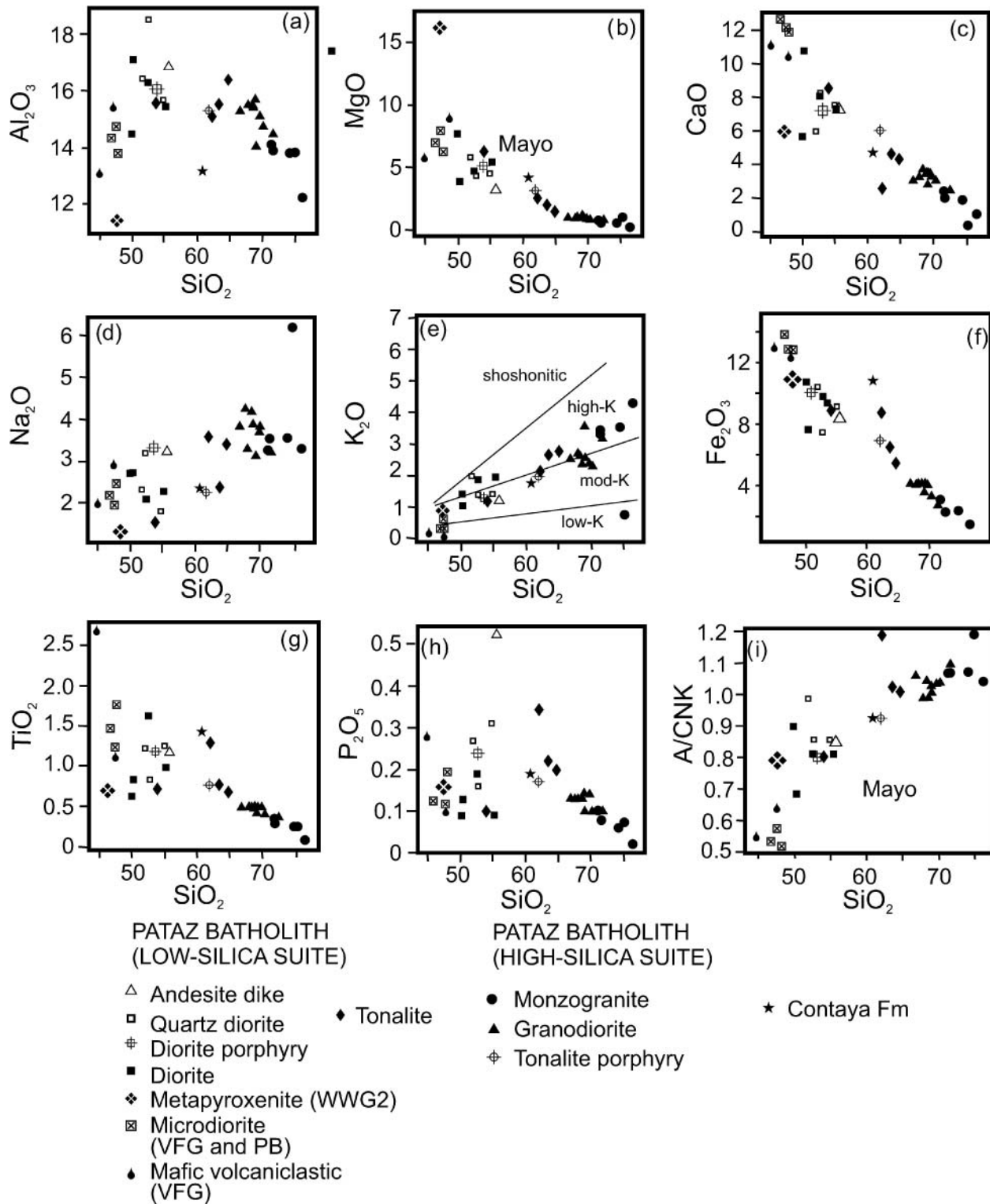


Figure 9 Harker variation diagrams (major elements), Pataz batholith. (a) Al_2O_3 , (b) MgO , (c) CaO , (d) Na_2O , (e) K_2O , (f) Fe_2O_3 , (g) TiO_2 , (h) P_2O_5 and (i) A/CNK . VFG is Vista Florida Group. Subdivisions in (e) after Pecerrillo & Taylor (1979).

poor correlation between $(\text{La}/\text{Yb})_{\text{N}}$ and SiO_2 . Both suites show pronounced positive Pb anomalies on multi-element spidergrams normalised to an NMORB composition, but these are higher in the low- SiO_2 suite and highest in WWG24 and WWG28 (Figure 8b, c). Most low-silica suite samples display strong enrichment of the incompatible elements (e.g. Cs, Rb, Ba, Th, U, K), and

weak negative P (\pm Sr) anomalies, but any Ti anomaly is minor or absent (Nb was not analysed). The most primitive samples of the low SiO_2 suite (e.g. WWG24 and WWG28) are less enriched in La, Ce, K, U (below detection) and Th than other samples, but are similarly enriched in Ba, Rb and Cs. The high-silica suite shows a more pronounced negative P (\pm Sr) anomaly and similar

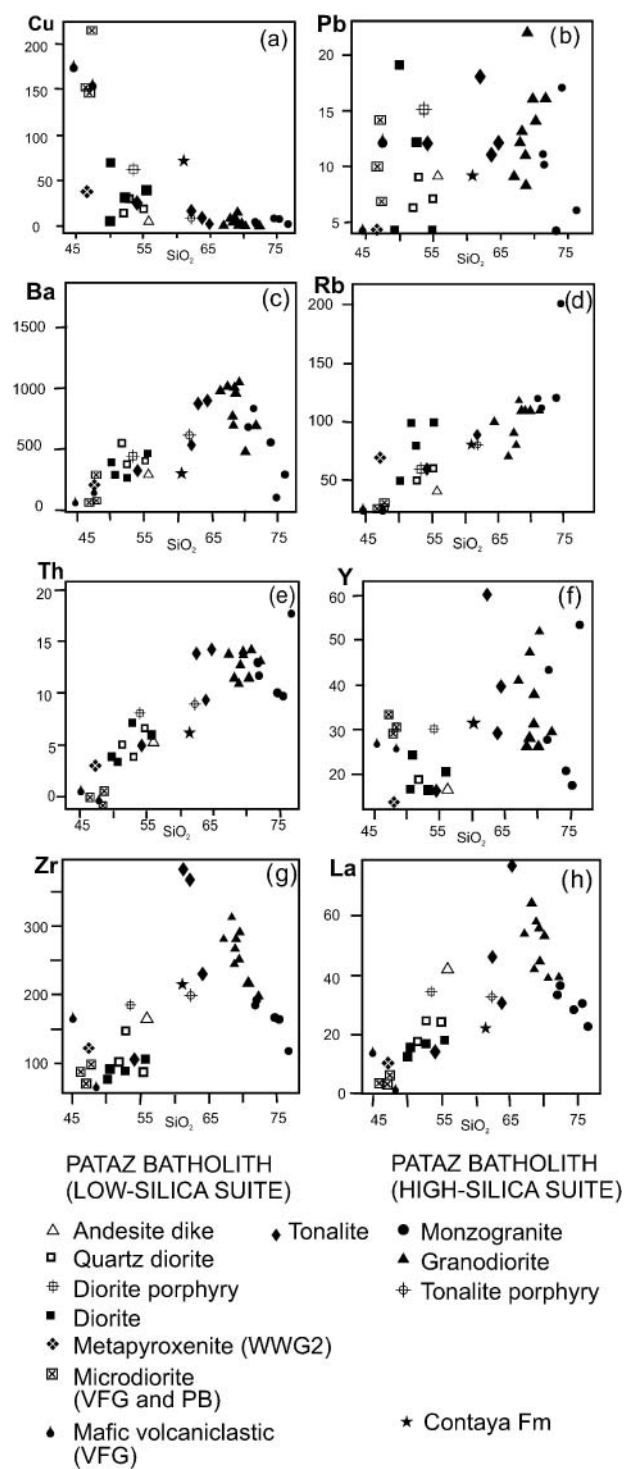


Figure 10 Harker variation diagrams (trace elements), Patata batholith. (a) Cu, (b) Pb, (c) Ba, (d) Rb, (e) Th, (f) Y, (g) Zr and (h) La. VFG, Vista Florida Group.

enrichment of incompatible elements, but stronger negative Ti anomalies (Figure 8b). Two samples, not the most primitive of the group, define a negative Ba anomaly.

Geochemistry of the Esperanza–Lavasen suite

Felsic rocks of the Lavasen Volcanics and the Esperanza subvolcanic complex span the range 68.1 to 82.7 wt%

SiO₂ (Supplementary Papers Table A2) with the highest values clearly affected by hydrothermal alteration. Samples plot in the alkali-rich part of the calc-alkaline field on an AFM diagram (Figure 4a), and are mildly to distinctly peraluminous according to the A/CNK ratio (Figure 4b). The more peraluminous compositions of some Lavasen samples may have been influenced by hydrothermal alteration, in which case most samples have A/CNK ratios ≤ 1.1 . Apart from one K-depleted sample of Lavasen Volcanics (silicified sample 206773 with 82.7 wt% SiO₂), all samples plot in the high-K calc-alkaline series field on an SiO₂ vs K₂O plot (Figure 4c). The samples are subalkaline and plot in the rhyolite and rhyodacite/dacite fields on a Zr/TiO₂ vs Nb/Y diagram (Figure 5a). Two anomalous samples of latite porphyry (samples 195022 and 195026) that plot within the rhyodacite/dacite field are less silicic than the bulk of the Esperanza–Lavasen suite, and these samples plot away from the rest of the samples in most other geochemical plots. On plots developed by Frost *et al.* (2001), the Lavasen Volcanics and the Esperanza subvolcanic complex samples are distinctly ferroan, and most samples plot within the high alkali part of the calc-alkalic association (Figure 6).

Apart from latite porphyry samples 195022 and 195026, the Esperanza and Lavasen samples are tightly clustered on plots incorporating V, Th and Zr, which effectively distinguish the two groups, and also distinguish the Lavasen and Esperanza samples from the Atahualpa and Vijus formations samples (Figure 5c). The Lavasen samples have a slightly higher Th/Zr ratio than the Esperanza samples, even though these two groups overlap on most other plots (e.g. Figures 4, 5a,b). Similar triangular plots to Figure 5c show that the Lavasen Volcanics also have a slightly higher Hf/Zr ratio than the Esperanza latitic rocks.

Potential mobility of silica (SiO₂) requires the use of an alternative parameter to monitor the degree of fractionation within the Esperanza and, more especially, Lavasen sample groups. The parameter chosen for this purpose is mg# (moles MgO/moles MgO + moles Fe₂O₃; Fe₂O₃ is an expression of total Fe). Using mg# is preferable to using SiO₂ to monitor fractionation but introduces its own problems. In particular, sample 206773 contains very low Fe₂O₃ and consequently has a high mg# that is difficult to reconcile with the felsic appearance of the sample in the field and thin-section. This sample also shows evidence of silicification (82.7 wt% SiO₂) and may have lost Fe as a result of hydrothermal alteration. The immobile trace-element character of this sample suggests it is an altered rhyolite similar to other felsic Lavasen Volcanic samples (Figure 5a).

Assuming sample 206773 is a rhyolite with a pre-alteration mg# similar to other rhyolites, Lavasen Group felsic samples have a more restricted range of mg# compared with the Esperanza subvolcanic complex, but generally overlap with the more felsic members of the latter (Figures 11, 12). The extended compositional range of the Esperanza samples is caused by the two relatively mafic latite samples (195022 and 195026). These two samples are characterised by relatively high mg#, as well as elevated Al₂O₃, CaO, P₂O₅, MgO, Fe₂O₃, TiO₂, V and Co, but also Zr and Hf (Figure 12c, d, f). Interestingly, these two samples

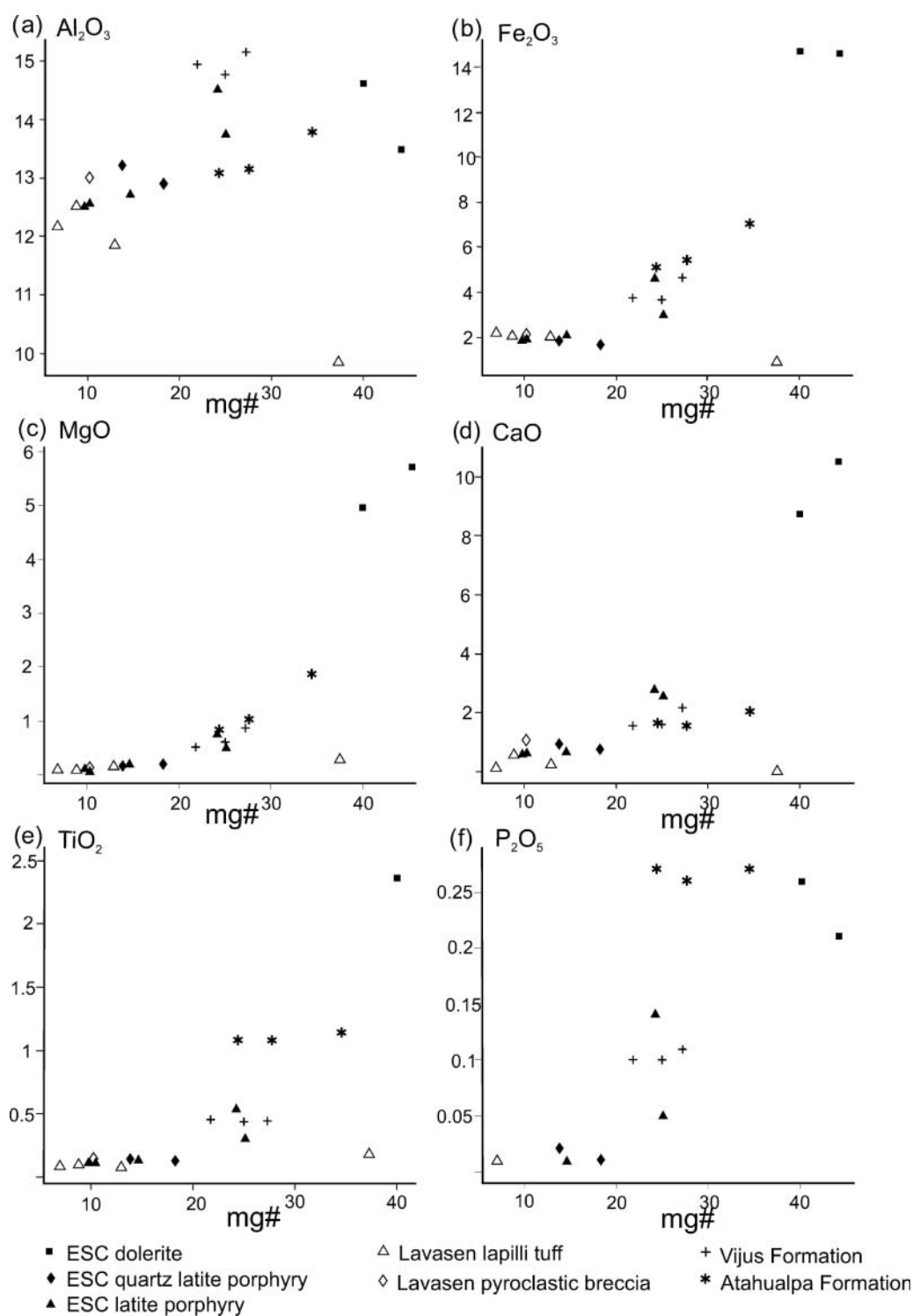


Figure 11 Variation diagrams showing major-element concentrations as a function of mg#, Esperanza–Lavasen samples, Vijus and Atahualpa samples: (a) Al₂O₃, (b) Fe₂O₃, (c) MgO, (d) CaO, (e) TiO₂ and (f) P₂O₅. mg#, moles MgO/moles MgO + moles Fe₂O₃; Fe₂O₃ is an expression of total Fe. Note one dolerite sample contains >2.5 (2.88) wt% TiO₂.

do not contain higher Ni and Cr than the rest of the Esperanza–Lavasen suite, although the absolute abundances are near the threshold of detection. Within the main group of samples (at mg# <20), Al₂O₃ decreases, and CaO, MgO, TiO₂ and P₂O₅ remain more or less constant, with decreasing mg#. There is little variation in the abundance of most trace elements with mg# (Figure 12).

REE patterns show that latitic rocks of the Esperanza subvolcanic complex are tightly grouped and characterised by flat HREE (Ho to Lu) and steep MREE to LREE, interrupted by a prominent negative Eu anomaly (Figure 7d). Lavasen Volcanic samples display similar REE patterns, except that the range of REE concentrations is displaced to slightly lower values, and the

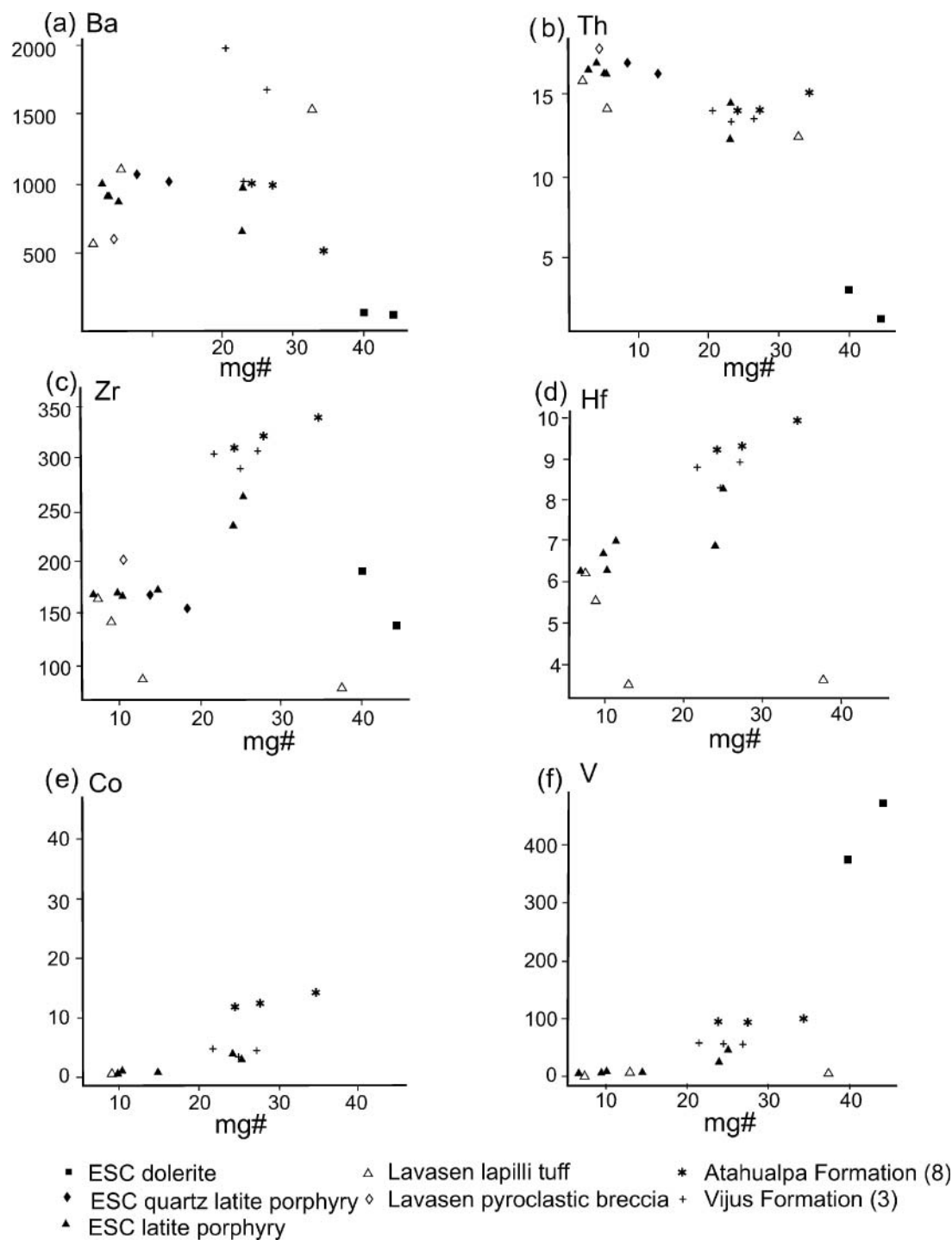


Figure 12 Variation diagrams showing trace-element concentrations as a function of mg#, Esperanza–Lavasen samples, Vijus and Atahualpa samples; (a) Ba, (b) Th, (c) Zr, (d) Hf, (e) Co and (f) V. mg# is moles MgO/moles MgO + moles Fe₂O₃; Fe₂O₃ is an expression of total Fe.

negative Eu anomalies are deeper (Figure 7e). For the Esperanza–Lavasen samples, the (La/Yb)_N ratios range between 3.62 and 8.68; (La/Sm)_N ratios range between 1.83 and 3.89. The Lavasen and Esperanza samples have very similar NMORB-normalised multi-element spidergrams characterised by deep, negative Nb, Sr–P and Ti anomalies and positive Pb anomalies (Figure 8d, e).

Two samples of dolerite from the Esperanza subvolcanic complex plot in the tholeiite field on an AFM

diagram (Figure 4a). Both samples plot as basalt on the Zr/TiO₂ vs Nb/Y diagram, but one sample plots in the subalkaline field and the other just within the alkaline basalt field (Figure 5a). The two samples display distinctive REE curves, much less fractionated than the associated latitic rocks and lacking Eu anomalies (Figure 7f). Spidergrams normalised to an NMORB composition are also relatively flat. Although most elements are 10× those of typical NMORB compositions, Rb and Cs are

strongly enriched ($\sim 100\times$ NMORB; Figure 8f). The spidergrams display a prominent positive Pb anomaly and a weak negative Ba anomaly.

Geochemistry of the Estrella monzonite porphyry

The monzonite porphyry sample from Estrella (near Santa Filomena in Figure 2) is clearly differentiated from the high-silica batholith suite and the Esperanza-Lavasen suite by virtue of its high K_2O (Figure 4c), Ba, Rb, Th, high total alkalis (Figure 6b) and high K_2O/Na_2O ratio (Figure 3c). This is the only sample that clearly plots in the shoshonitic field on Figure 4c. As for the Esperanza-Lavasen suite, relatively high K, Ba and Rb in this intrusion is consistent with petrographic evidence for early crystallisation of K-feldspar. The REE curve for the Estrella monzonite porphyry (WWG11) is very similar to those of Esperanza subvolcanic complex latites but at the upper end of the range (Figure 7d). The spidergram is also similar in form to those of the Esperanza subvolcanic complex but is relatively enriched in Ba and Rb, and depleted in Pb, Zr, Y and the REE (Figure 8d).

DISCUSSION

Petrogenesis of the Vijus and Atahualpa formations

The LREE-enriched REE curves and enrichment of incompatible elements on chondrite- and NMORB-normalised spidergrams, respectively, are features typical of moderate- to high-K calc-alkaline magmas from continental arc environments (Pearce 1983; Wilson 1989). The negative Nb and Ti anomalies (Pearce 1983, 1996; Jenner 1996) and positive Pb anomalies (Elliott *et al.* 1997) are also typical features of island and continental arc rocks. These types of magmas are generally considered to be generated in the metasomatised mantle wedge, above subduction zones (Pearce 1983; Wilson 1989) with the negative Nb anomaly reflecting a previous melt extraction event in the source region and addition of low volume melts enriched in large ion lithophile elements (LILE) and LREE (McCulloch & Gamble 1991). Although the overall form of the spidergrams is similar to that of calc-alkaline magmas, the degree of enrichment of all elements, especially the alkalis and LREE is high compared with typical continental arc basalts (Figure 8a), and more comparable to those erupted on thick continental lithosphere (Pearce 1983) or the 'mature continental arcs' of Brown *et al.* (1984). The relatively felsic bulk composition of the volcanic rocks, particularly the Vijus Formation (Figure 9a), and the prominent negative Eu and Sr anomalies (Figures 7a, 8a), and low Cr (<50 ppm) and Ni (<20 ppm) suggest a role for plagioclase fractionation and indicate that these are not pristine mantle melts. The Vijus and Atahualpa magmas could have been generated in metasomatised asthenosphere or subcontinental lithosphere and attained their more felsic compositions through fractional crystallisation and/or crustal assimilation. Alternatively, they may have formed more directly by partial melting of the lower continental crust, providing the source had an appropriate (andesitic)

composition inherited from an earlier period of subduction (e.g. Chappell & Stephens 1988). Additional whole-rock isotopic data are required to allow a distinction between these processes. The presence of Mesoproterozoic zircon xenocrysts in the Atahualpa Formation (Witt *et al.* 2013a) does not provide critical evidence for either argument because these could be interpreted as restite carried from the lower crustal source or refractory components of a crustal contaminant. Miskovic & Schaltegger (2009) describe the Vijus Formation as andesitic, which suggests that the felsic rocks in the Pataz district may be a minor component of the regional volcanic sequence. Therefore, we favour an origin for the Vijus and Atahualpa formations as fractionation products of subduction-related arc magmas with a metasomatised mantle or subcontinental lithosphere source. A significant component of fractional crystallisation as indicated by elevated Ba (500–2000 ppm), Th (13–16 ppm) and Zr (280–340 ppm) (Figure 12) and depleted Sr and P (Figure 8a) may also be attributed to fractional crystallisation.

Atahualpa Formation volcanoclastic rocks contain higher Fe_2O_3 , MgO, TiO_2 , P_2O_5 , Zr, Th, V, Ni, Co and Cr, but lower Al_2O_3 and Ba, than Vijus Formation samples (Figures 11, 12). They are probably not related to Vijus Formation volcanics by fractional crystallisation, as they tend to plot in separate clusters on variation diagrams and in ternary diagrams such as Figure 5c, and are separated stratigraphically by the metasedimentary Contaya Formation (Haeberlin *et al.* 2004; Witt *et al.* 2013a). Compositional differences may reflect different source compositions and/or degrees of crustal contamination for the Vijus Formation.

Petrogenesis of the low- SiO_2 suite of the Pataz batholith and Vista Florida Group

The depleted LREE patterns of least evolved samples WWG24 and WWG28 from the low- SiO_2 batholith suite resemble those for tholeiitic NMORB basalts, and these two samples plot in the tholeiitic field of an AFM diagram (Figure 4a). However, the NMORB-normalised spidergrams for these samples display pronounced enrichment of Cs, Rb and Ba, and more modest enrichment of K and Th, as well as a pronounced positive Pb anomaly. This suite of enriched elements is generally believed to be derived from the subducted sedimentary layer in oceanic subduction zone settings (Pearce 1982, 1983; Elliott *et al.* 1997). In contrast to most continental subduction zone magmas (Pearce 1982, 1983; Brown *et al.* 1984), LREE, MREE and Zr are not enriched in these primitive members of the low- SiO_2 batholith suite. Furthermore, although the absence of an Nb anomaly cannot be explicitly demonstrated (because Nb analyses are not available), the absence of a Ti anomaly contrasts with typical continental arc magmas (Pearce 1982, 1983; Brown *et al.* 1984). The absence of negative Ti anomalies on NMORB-normalised spidergrams suggests that the parent magma of the low- SiO_2 suite may not have arisen from a typical continental arc source region (i.e. the metasomatised asthenospheric wedge, Wilson 1989; or subcontinental lithosphere, Pearce 1983). According to the model of McCulloch & Gamble (1991), this could

mean that the mantle source for the low-SiO₂ suite had not been depleted by a previous melting event. Nevertheless, even the most primitive of low-SiO₂ samples (WWG24, WWG28) display enrichment in alkalis and Th, and a prominent positive Pb anomaly, suggesting that the mantle source had been metasomatised, probably by low-volume melts derived from the slab or deeper parts of the asthenospheric mantle. The Cr and Ni concentrations in the low-SiO₂ suite samples are well below those predicted for primary mantle-derived melts (900 ppm and 350 ppm, respectively; Cox *et al.* 1980) indicating that the parent magma had evolved, probably by fractional crystallisation and/or crustal contamination, since initial formation in the mantle source region.

Other samples of the low-SiO₂ batholith suite display pronounced enrichment of LREE (La and Ce are 10× to 100× chondrite values), Th and U, and modest enrichment of Nd, Sm and Zr, and a positive Pb anomaly (Figure 8c). Compared with WWG24 and WWG28, these samples are further enriched in K, Th, U, LREE, P, Nd, Sm and Zr but are depleted in HREE and Y. The resulting spidergrams for evolved low-SiO₂ samples are similar to those of the Vijus and Atahualpa formations and other high-K calc-alkaline magmas from continental arcs on thick lithosphere (Brown *et al.* 1984; Wilson 1989; Price *et al.* 1999). Compositional variation within the low-SiO₂ suite could be explained by contamination or assimilation of magma similar to that which produced WWG24 and WWG28, by continental crust containing elevated alkalis, LREE, Th, U and P, but similar Pb, lower HREE and Y than the parent low-SiO₂ magma. Mesoproterozoic rocks in the central segment of the Eastern Andean Cordillera reported by Miskovic & Schaltegger (2009) and Miskovic *et al.* (2009) have the appropriate composition to cause this contamination.

The negative correlation of MgO, CaO and Fe₂O₃ and V (total) with increasing silica is consistent with assimilation of crustal material with higher SiO₂ than the parent low-SiO₂ magma, or fractional crystallisation. However, trace elements such as Sr and Ti do not demonstrate a regular negative correlation against alkali elements, as would be expected of fractional crystallisation. Fractional crystallisation of clinopyroxene and amphibole would be expected to produce steep enrichment trends for Zr, similar to that defined by other incompatible elements such as Th and Rb (Figure 10). The weak enrichment trends for Zr are consistent with assimilation of material with much higher Rb and Th but only slightly higher Zr, as is the case for the Mesoproterozoic crust beneath the Eastern Andean Cordillera (Miskovic & Schaltegger 2009; Miskovic *et al.* 2009). Therefore, fractional crystallisation is assigned a relatively minor role for compositional variation within the low-SiO₂ suite, most of which is attributed to variable assimilation of Mesozoic continental crust of heterogeneous but overall intermediate to felsic composition.

Petrogenesis of the high-SiO₂ Pataz batholith suite

The high-SiO₂ suite of the Pataz batholith, dominated by granodiorite (with subordinate monzogranite and tonalite), has the geochemical characteristics of calc-alkaline

I-type granites, as described by previous investigators (Schreiber *et al.* 1990; Macfarlane *et al.* 1999). The REE curves and NMORB-normalised spidergrams for high-SiO₂ batholith suite samples, incorporating high LREE/HREE ratios and enrichment of incompatible elements, are typical of mature continental arc magmas (Brown *et al.* 1984). The positive Pb anomaly seen in the Vijus and Atahualpa formations and the low-SiO₂ batholith suite is also present, although weaker; in the high-SiO₂ samples, caused mainly by relative enrichment of LREE and Sr (Figure 8b). A negative Ti anomaly on the NMORB-normalised spidergram (Figure 8b) is also a feature of calc-alkaline magmas in arc environments. Although Nb analyses are not available for the high-SiO₂ suite, Miskovic *et al.* (2009) also noted the presence of negative Nb anomalies in their regional study of Permian–Carboniferous granitoids of the Eastern Andean Cordillera.

As for other calc-alkaline, I-type granodiorite-dominated suites, the Pataz high-SiO₂ suite melt is interpreted to have formed by partial melting of an older Cordilleran-type andesite or diorite source in the lower crust (cf. Chappell & Stephens 1988; Chappell & White 1992), consistent with the radiogenic Pb and Nd isotopes reported by Macfarlane *et al.* (1999) and, more generally, with the Lu–Hf isotope data of Permian–Carboniferous granitoids in the Eastern Andean Cordillera (Miskovic *et al.* 2009). The partly contemporaneous, mantle-derived low-SiO₂ magma probably provided the heat source required to melt the lower crustal source rocks.

Lead and Nd isotopic data (Macfarlane *et al.* 1999), and Lu–Hf isotope data (Miskovic & Schaltegger 2009) indicate that felsic crustal material played an important role in the chemistry of the Pataz batholith and associated dykes. This conclusion is consistent with the model presented here, which derives the Pataz batholith granodiorite from melting of older, arc-related andesitic or dioritic source rocks in the lower crust. Possible candidates for this andesitic crust are the Mesoproterozoic San Ignacio-Sunsas orogen, and equivalents of the Vijus and Atahualpa formation magmas that may have accumulated in the lower crust.

A distinct parent magma composition for the high-SiO₂ suite could not be recognised. Sample WWG7 (tonalite porphyry from Karola) has the lowest SiO₂ (61.9 wt%) and highest mg# (0.64) of all high-SiO₂ suite samples. Samples WWG26 and WWG31 have slightly higher SiO₂ (62.3 wt% and 64.8 wt%, respectively) and lower mg# (0.53 and 0.49, respectively). These three tonalite samples plot away from the main trend defined by high-SiO₂ suite samples, which otherwise define a depletion trend in Zr and LREE with increasing fractionation (Figure 10g, h).

Magma mingling structures (Miskovic *et al.* 2006, 2009; Witt *et al.* 2013a) warrant assessment of magma mixing between low- and high-silica suite magmas. Binary plots involving trace-element ratios should produce curved trends where compositional variation is caused by magma mixing (Cox *et al.* 1980). The Pataz batholith data plot along straight-line trends (Figure 13a, b) and are not consistent with magma mixing as a significant process leading to compositional variation. Magma mixing between low- and high-SiO₂ magmas is also inconsistent with the behaviour of Al₂O₃, P₂O₅, Ba, Zr, La

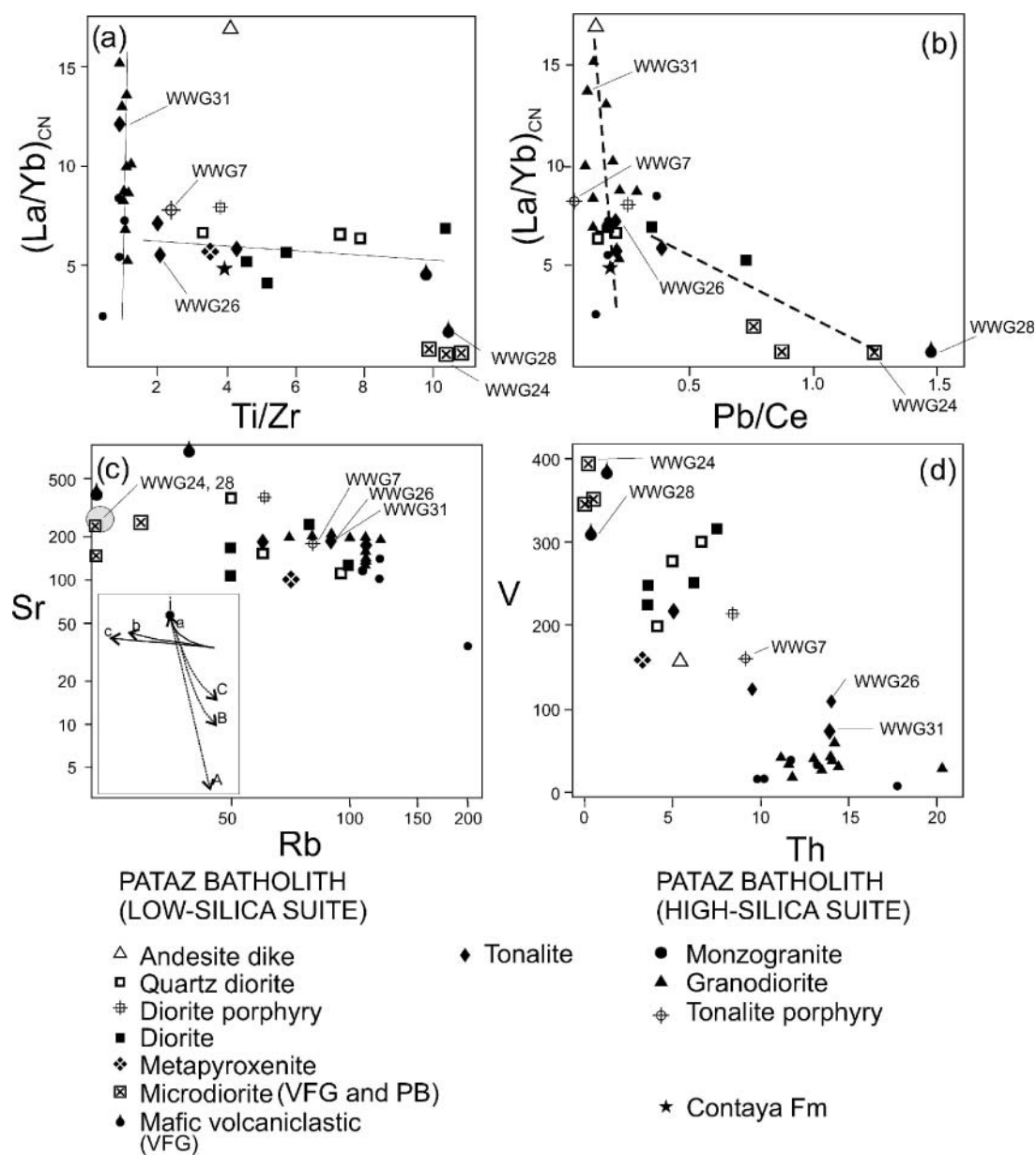


Figure 13 Trace-element plots to distinguish genetic processes for the Pataz batholith. Plots of $(La/Yb)_{CN}$ vs (a) Ti/Zr and (b) Pb/Ce . Magma mixing between two end-members should generate a curved array of data on these plots; the approximate straight-line relationship, especially in Figure 17a, is not compatible with magma mixing between the low- and high-silica suites. Log-log plots of Sr vs Rb (c) and V vs Th (d). Inset in (c) is applicable to (c, d) and presents the generalised form of trends defined by fractional crystallisation and partial melting (after Cocherie 1986). For fractional crystallisation, i is the initial composition of the magma; A is the compositional trend of the magma caused by fractional crystallisation; B and C are the compositional trends of the magma caused by incremental equilibrium crystallisation where increments of magma are removed after 10% (B) and 20% (C) crystallisation. For partial melting, i is the initial bulk composition of the source rock; a is the compositional trend of the magma caused by batch partial melting; c is the compositional trend of the magma caused by fractional partial melting with continuous removal of the melt; b is an intermediate process between perfect batch melting and perfect fractional melting. Compositions of least fractionated (closest to starting composition) samples WVG24, WVG28 and WVG31 are shown; WVG24 and WVG28 contain <10 ppm Rb and are not plotted as individual points, but the area in which they would plot is shown as a grey circle.

and Ce (Figures 9, 10). It can therefore be concluded that any mixing or assimilation between mantle-derived and crustal magmas took place in the source region and helped define the composition of the parental high-SiO₂ magma.

Harker variation diagrams suggest a role for fractionation within the high-silica suite (Figures 9, 10).

Depletion of MgO, TiO₂, Fe₂O₃ (total), CaO, Ni, Co, V and Sc with increasing SiO₂, and negative Eu anomalies, in the high-silica suite are consistent with fractionation of amphibole, plagioclase and biotite. Depletion of Zr and LREE with increasing SiO₂ (Figure 10g, h) is attributed to fractionation of accessory phases such as zircon and apatite, the latter supported by negative P anomalies on

NMORB-normalised spidergrams (Figure 8b). The term fractionation, as applied here, could refer to fractional crystallisation of the magmas (during ascent or following emplacement), or variable partial melting within the source region. Log-log plots using compatible and incompatible trace elements can be used to assess the relative roles of these processes (Cocherie 1986). The relatively flat trends shown by the Patáz data on log-log plots involving Sr and V (compatible elements) and Rb and Th (incompatible elements) are not consistent with extended fractional crystallisation, whereby compatible elements are rapidly depleted, but could be explained by equilibrium crystallisation and/or variable batch partial melting (Figure 13c, d; Cocherie 1986). Rapid depletion of Zr and LREE may indicate a role for fractional crystallisation, but the data suggest that variable partial melting of continental crust dominated compositional variation within the high-SiO₂ suite. Some variation in the proportion of crustal and mantle-derived magmas in the source region may also have contributed to compositional variation among batches of parental high-SiO₂ magma. A fractional crystallisation relationship between the low-silica suite and the high-silica suite is precluded by the silica gap between 55 and 60 wt% SiO₂ and the contrasting behaviours of Al₂O₃, P₂O₅, Ba, Zr, La and Ce (Figures 9, 10).

Data presented here for the Patáz batholith display weak and inconsistent convergence towards the sample of Contaya Formation on plots involving major and trace elements (Figures 9, 10). Although only one sample has been analysed, it is taken from the immediate country rock of the batholith and incorporates several inter-beds of sandstone and siltstone and is believed to be reasonably representative of the Contaya Formation, which is a fairly uniform sequence of sedimentary rocks in the Patáz district. The plots in Figures 9 and 10 suggest that assimilation of metasedimentary country rock has not had a major influence on the geochemistry of the Patáz batholith, despite the widespread presence of accidental xenoliths.

Petrogenesis of the Esperanza–Lavasen association and the Estrella monzonite porphyry

The Fe-rich Esperanza dolerite crystallised from a tholeiitic parent magma (Figure 4a). The relatively flat REE patterns (Figure 7f) are similar to those of basalts derived from slightly to moderately enriched EMORB mantle sources (Pearce 1983; Wilson 1989) but are approximately 10× more enriched than average MORB (Figure 8f). The tendency towards alkaline compositions (Figure 5a) suggests that these mafic magmas were produced by relatively small volume partial melting of a metasomatised mantle source, possibly at greater depths than the source for low-SiO₂ suite batholith magmas (Jaques & Green 1980). The 10× enrichment of Y and Yb, and most other elements, relative to average MORB (Figure 8f) also suggests small volume partial melting of the mantle source. Although REE curves and spidergrams are flat compared with other igneous rocks in the Patáz district, both dolerite samples display the positive Pb anomalies and enrichment of Cs and Rb suggesting the doleritic magma was produced by partial melting of

a compositionally similar mantle source to that which yielded the least evolved low-SiO₂ batholith samples (i.e. a metasomatised mantle source). Also, the absence of negative Nb anomalies suggests this mantle source had not previously been depleted by partial melt extraction (McCulloch & Gamble 1991). The Mg#, Ni and Cr contents of the dolerites indicate that they are not primary mantle-derived melts, but the absence of negative Eu anomalies on REE curves precludes significant fractionation of plagioclase. Fractional crystallisation, which probably caused the iron-rich composition of the dolerites, was likely dominated by olivine and pyroxene.

Compared with the Patáz batholith, latitic to rhyolitic rocks of the Esperanza–Lavasen felsic suite are distinctly ferroan and alkali-rich (Figure 6). These qualities identify the Esperanza–Lavasen felsic samples as having affinities with A-type or anorogenic felsic magmas (cf. Eby 1990; Frost *et al.* 2001). The A-type character of the samples is supported by plots developed by Dall'Agnol & de Oliveira (2007), which show that the Esperanza–Lavasen samples plot with moderately oxidised anorogenic granites (Figure 14a, b). The low CaO and Al₂O₃, and high K₂O and Fe_{TOT}/MgO, shown by the Esperanza–Lavasen felsic samples are characteristic of A-type magmas, as are the Fe-rich compositions of amphibole (inferred from the deep green colour) and relict pyroxene (Anderson 1983; Whalen *et al.* 1987; Eby 1990; Pitcher 1997; Dall'Agnol & de Oliveira 2007). The plots in Figures 6 and 14 are based on major elements, some including alkalis, which may have been susceptible to hydrothermal alteration. However, supporting arguments for an A-type classification are based on immobile trace element plots, such as those developed by Whalen *et al.* (1987). For example, on a FeO_{TOT} vs 1000Ga/Al plot, all latitic samples (excluding the two most mafic Esperanza samples: 195022 and 195026) fall in the field of A-type granites (Figure 5b). Elevated high-field-strength element concentrations are a characteristic feature of A-type magmas (Eby 1990; Pitcher 1997; Dall'Agnol & de Oliveira 2007), and the Esperanza–Lavasen samples are generally enriched in Zr, Ta, Th and LREE compared with the Patáz batholith (Figure 8; Supplementary Papers Table A2). The REE curves of the Esperanza–Lavasen felsic suite are also very similar to those of the A-type quartz latite-granitoid suite from the Roxby Downs area, South Australia (Creaser 1996), which hosts the Olympic Dam Cu–Au–U–REE deposit.

The large volume of Lavasen Volcanics (at least 2000 km³) and the felsic nature of both the volcanic rocks and the Esperanza subvolcanic complex (including the very low Cr and Ni) imply a crustal source for the magmas, consistent with Y/Nb ratios >1.2 (Eby 1990). Models for the origin of A-type magmas include second melting of a residual source that had previously yielded a calc-alkaline I-type melt (Collins *et al.* 1982) and low pressure melting of a calc-alkaline (tonalitic to granodioritic) source (Creaser *et al.* 1991; Roberts & Clemens 1993; Dall'Agnol & de Oliveira 2007), as well as fractionation of a tholeiitic magma (Turner *et al.* 1992; Frost & Frost 1997). Despite the close spatial and temporal association of the Esperanza–Lavasen suite with the I-type Patáz batholith and its residue in the lower crust, first-stage melting of a tonalitic to granodioritic source is preferred

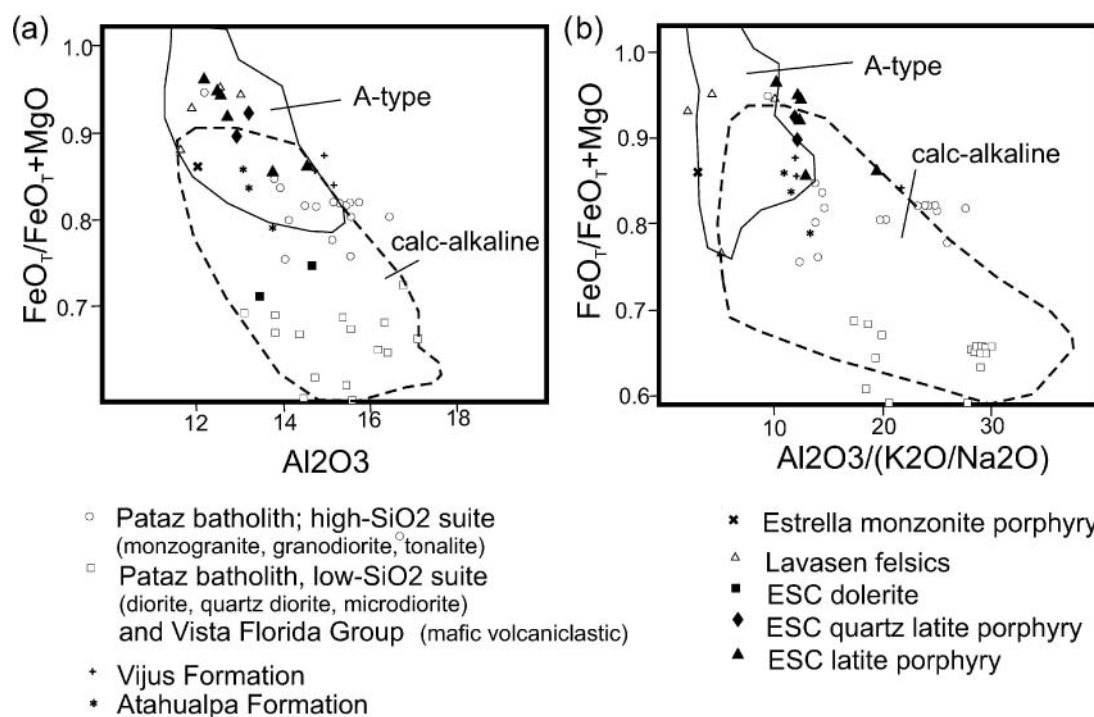


Figure 14 Plots used for distinguishing Esperanza–Lavasen samples from Pataz batholith samples. (a) $\text{FeO}_{\text{TOT}}/(\text{FeO}_{\text{TOT}} + \text{MgO})$ vs Al_2O_3 and (b) $\text{FeO}_{\text{TOT}}/(\text{FeO}_{\text{TOT}} + \text{MgO})$ vs $\text{Al}_2\text{O}_3/(\text{K}_2\text{O} + \text{Na}_2\text{O})$ as recommended by Dall’Agnol & de Oliveira (2007) for the distinction and classification of A-type granites. Calc-alkaline and A-type fields from Frost *et al.* (2001).

for reasons outlined by Creaser *et al.* (1991). In either case, high-temperature partial melting probably requires thermal input from a mantle-derived magma emplaced into the source region. The Fe-rich dolerite dykes post-date latitic rocks of the Esperanza subvolcanic complex, but their presence shows that mantle-derived magma may have been present in the crustal source region to provide the required heat. Fractionation in this inferred tholeiitic magma chamber could have given rise to the A-type Esperanza and Lavasen magmas, but we have no evidence at the present level of erosion to suggest this occurred.

It was noted above that most Esperanza–Lavasen felsic samples plot within the A-type field in Figure 5b, but two samples (195022 and 195026) do not. These two samples have the lowest SiO₂ and the highest CaO, MgO, FeO_T, MnO, TiO₂, P₂O₅ and MgO/Fe₂O₃ ratio, indicating they are less evolved than the other samples. Most samples plot within a restricted range in mg# (0 to 20), but inclusion of samples 195022 and 195026 extends the range into the mid 20s. A crudely stratified magma chamber is envisaged for the mid-crustal source region of the Esperanza–Lavasen felsic suite, comprising a lower, mantle-derived mafic melt and an upper, crustal melt of felsic A-type composition (cf. Barnes 1983; Sparks *et al.* 1984). The relatively mafic composition of samples 195022 and 195026 are interpreted to result from mixing of mantle-derived and crustal melts across a transitional zone within this lower crustal magma chamber, prior to eruption. The Fe-rich dolerites are probably not representative of the lower, mafic magma in the hypothesised magma chamber because samples 195022 and 195026 do not lie on a mixing line between the Fe-rich dolerites

and the latitic rocks (Figures 11, 12; see particularly Zr and Hf).

The remaining latitic samples of the Esperanza subvolcanic complex and those of the Lavasen Volcanics more likely represent unmodified melt derived from the upper part of the magma chamber, where crustally derived magma predominated. A more potassic, felsic (tonalite or granodiorite) source than that which produced the Pataz granodiorite is implicated (Chappell & Stephens 1988; Roberts & Clemens 1993). Similar to the source for the Pataz granodiorite, the positive Pb anomaly and some of the enrichment in Cs and Rb may have been inherited from this lower crustal source. This source rock must also have had negative Ti and Nb anomalies, inherited from the calc-alkaline source rocks in the mid crust. A suitable source for the Esperanza–Lavasen A-type magma is the compositionally variable Mesoproterozoic basement (e.g. the Satipo Tonalite) reported by Miskovic *et al.* (2009) and Miskovic & Schaltegger (2009), or possibly mid-crustal equivalents of the high-SiO₂ Pataz batholith suite.

The Estrella monzonite porphyry (near Santa Filomena in Figure 2) shows petrographic similarities to the Esperanza–Lavasen felsic suite, especially the presence of K-feldspar phenocrysts. The intrusion has the highest alkali content of all intrusions investigated in the Pataz district and is the only one to plot clearly within the shoshonite field in Figure 4c. A similar origin by partial melting of mid-crustal tonalite or granodiorite is proposed. However, the age of the Estrella monzonite porphyry is largely unconstrained following the failure of SHRIMP U–Pb dating of zircon to identify an unequivocal emplacement age (Witt *et al.* 2013a).

Tectonomagmatic evolution of the northern Pataz district

Previous geochronological and geochemical studies of granitoids in the Eastern Andean Cordillera of Peru have shown that this mainly Paleozoic belt represents a long-lived (up to 1.15 Ga) continental margin along the western edge of the Amazonia craton (Figure 1; Petersen 1999; Chew *et al.* 2007; Miskovic *et al.* 2009). Following the break-up of Rodinia in the Neoproterozoic (770–570 Ma), the history of the Eastern Andean Cordillera was characterised by almost continuous subduction, lasting into the late Triassic (Chew *et al.* 2007; Miskovic *et al.* 2009). The subduction zone setting of the Andean margin continues into the present, but the present locus of arc magmatism has shifted into the Western Andean Cordillera (Noble & McKee 1999; Petersen 1999). This study of igneous rocks in the northern Pataz district of the Eastern Andean Cordillera shows that intermediate to felsic magmas with arc-related continental margin geochemical signatures were emplaced into the Andean crust during the early Paleozoic (Vijus and Atahualpa formations) and Mississippian (Pataz batholith and Esperanza–Lavasen suite). The resulting volcanic and intrusive rocks consistently display alkali (Rb, Cs) enrichment, positive Pb anomalies, and most of the more felsic rocks exhibit a negative Nb anomaly or, where Nb is not available, a negative Ti anomaly (Figure 8). However, we contend that the more voluminous felsic Carboniferous magmas were generated by partial melting of the lower to mid-continental crust and inherited their continental arc signature from an earlier period of subduction, possibly that which produced the Vijus and Atahualpa formations during the Ordovician. This interpretation is consistent with the whole-rock chemistry discussed above and with the conclusions of Miskovic & Schaltegger (2009) who found a predominantly crustal Lu–Hf signature for Permian–Carboniferous granitoids in the Eastern Andean Cordillera of northern Peru. It is also consistent with the Pb and Nd isotope data of Macfarlane *et al.* (1999) who estimated a Mesoproterozoic crustal component of up to 70% for the Pataz batholith.

The origin of relatively primitive mafic intrusive rocks in the Pataz district (WWG24 and WWG28 of the low-SiO₂ batholith suite, and the Esperanza dolerites) is problematic. They display enrichment of alkalis Cs, Rb (\pm Ba) and a prominent positive Pb anomaly, and Mg#, Cr and Ni values consistent with fractionated partial melts derived from a mantle source that was metasomatised by fluids derived from subducted oceanic crust and sediments. However, the dolerites at least lack the characteristic negative Nb anomaly of arc-related magmas, and the low-SiO₂ batholith suite lacks a Ti anomaly, both of which may indicate that the mantle source had not previously been subject to partial melt extraction (McCulloch & Gamble 1991). If the Vijus and Atahualpa formation magmas, which incorporated a negative Nb anomaly, were formed by partial melting of mantle that had previously yielded a partial melt, the source region would have had to be replaced by undepleted asthenosphere before it melted again to produce the low-SiO₂ batholith and Esperanza dolerite magmas. Mechanisms that might induce this history include periodic upwelling

in incipient rifts and slab tears (Hale *et al.* 2009). Some of these mantle-derived magmas probably provided the thermal energy required to melt the continental crust and produce the Carboniferous felsic magmas.

The interpreted Ordovician to Mississippian tectonic evolution of the Andean margin in the vicinity of the northern Pataz district is summarised schematically in Figure 15. The volcanic rocks of the Atahualpa Formation are mid-Ordovician (SHRIMP U–Pb in zircon age = 466.8 ± 8.1 Ma; Witt *et al.* 2013a) and are stratigraphically younger than the rocks of the Vijus Formation, which is probably late Cambrian or Early Ordovician. The age of the Atahualpa Formation is coincident with the age obtained from zircons in the Esterella monzonite porphyry (Witt *et al.* 2013a), which may represent a feeder to the Cambrian–Ordovician volcanic rocks in the northern Pataz district. Ordovician igneous rocks are not common in the Andean margin of northern Peru, but the Sitabamba granodiorite gneiss, about 50 km south of Pataz in the Eastern Andean Cordillera, has a slightly younger age of *ca* 448.3–441 Ma (Chew *et al.* 2007; Miskovic *et al.* 2009). Chew *et al.* (2007) and Miskovic *et al.* (2009) interpreted the Vijus Formation andesites as part of a late Cambrian arc related to the accretion of the Paracas–Arequipa Terrane. A subsequent hiatus in magmatic activity, coincident with deposition of the Contaya Formation, is placed in the interval 460–450 Ma by Miskovic *et al.* (2009), but this is inconsistent with our mid-Ordovician SHRIMP age for the overlying Atahualpa Formation. The mid-Ordovician age for the Atahualpa Formation suggests that Atahualpa Formation volcanism is related to renewal of subduction in a zone located west of the accreted Paracas–Arequipa Terrane (Figure 15a; cf. Miskovic *et al.* 2009). Paleoproterozoic and Mesoproterozoic xenocrysts in the Atahualpa Formation suggest some contamination of arc magmas by lower continental crust formed by the Amazonia craton and the San Ignacio–Sunsas orogen, respectively. These Ordovician igneous rocks may be the northward continuation of the early Paleozoic San Nicolas–Famatina arc exposed in southwestern Peru and the Sierras Pampeanas in northwest Argentina (Bahlberg & Herve 1997; Miskovic *et al.* 2009).

During the mid-Mississippian (*ca* 338–336 Ma), the high-SiO₂ (mainly granodiorite) magma of the Pataz batholith formed as a result of partial melting of an andesitic or dioritic lower crustal source, and was emplaced in the mid- to upper crust (estimated a depth of 11 to 13 km; Haeberlin *et al.* 2004). A crustal source is indicated by the felsic bulk composition of the high-SiO₂ magma and geochemical data that point to variable partial melting rather than fractional crystallisation as the dominant genetic process. Positive Pb anomalies, enrichment of Cs and Rb, and implied negative Nb anomalies on NMORB-normalised spidergrams (Figure 8) are consistent with an arc-derived andesitic source in the lower continental crust. It is possible that the andesitic source was formed by the same magmas that formed the Vijus and Atahualpa formations but were underplated onto the base of the continental crust. Alternatively, the Mesoproterozoic San Ignacio–Sunsas orogen may again have provided the source. There are no xenocryst age data for the Pataz batholith known to the authors, but

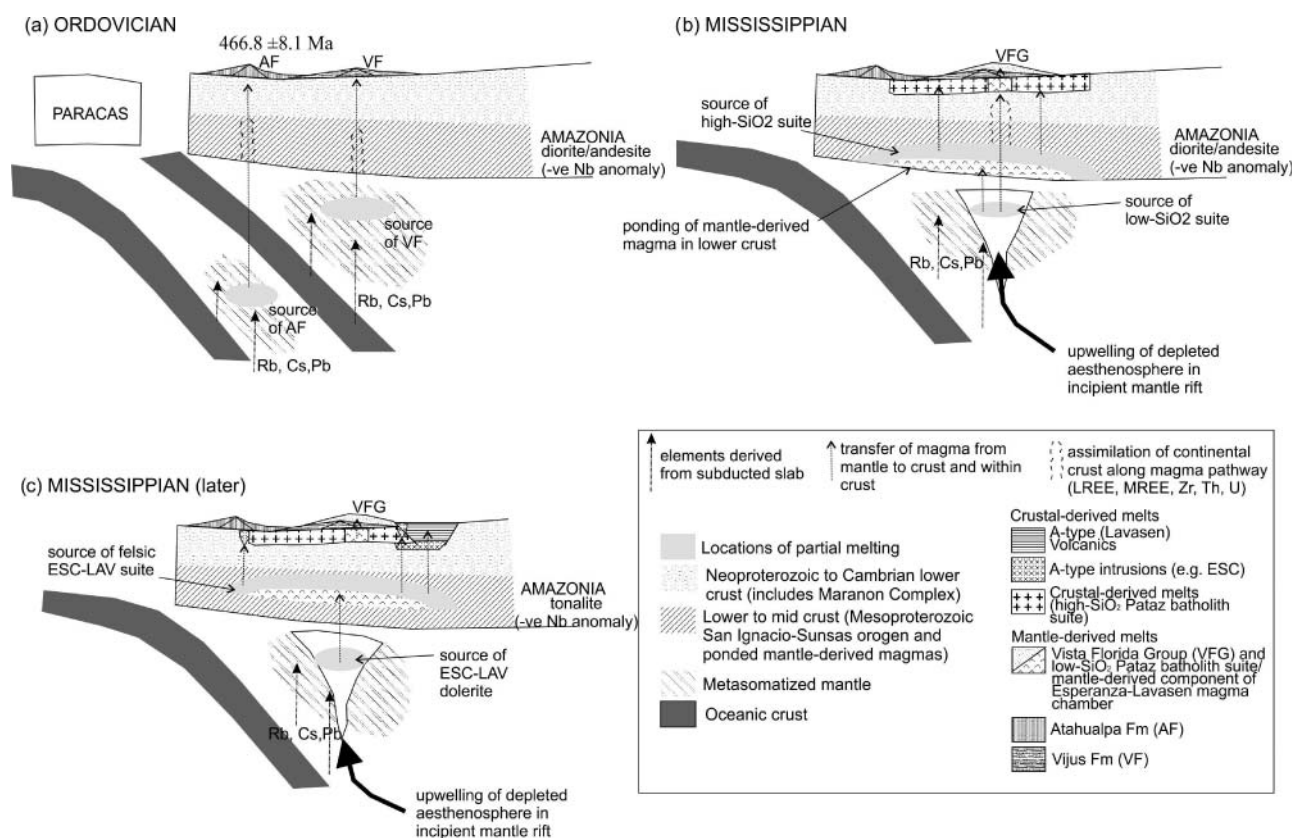


Figure 15 Schematic diagram summarising tectono-magmatic evolution of Pataz district during the Ordovician and Mississippian. (a) Deposition of Vijus and Atahualpa volcanics, derived by partial melting of metasomatized depleted mantle followed by fractionation and assimilation of lower continental crust; the Vijus Formation formed as the Paracas terrane docked with western Amazonia; the Atahualpa volcanics formed later, after subduction stepped outboard of the Paracas terrane; the Paracas terrane was removed by strike-slip deformation before the Mississippian (Miskovic *et al.* (2009)). (b) Mississippian melting of metasomatized undepleted mantle followed by assimilation of continental crust to produce Vista Florida volcanics and low-SiO₂ magmas of Pataz batholith; ponding of mantle melt causes melting of dioritic to andesitic continental crust to produce high-SiO₂ magmas of Pataz batholith. (c) Ponding of metasomatized, undepleted, mantle-derived magmas in tonalitic middle crust causes partial melting to produce A-type magmas of the Lavasen Volcanics and Esperanza subvolcanic complex.

Miskovic *et al.* (2009) report Mesoproterozoic xenocrysts from the Pennsylvanian (upper Carboniferous) Balsas granodiorite 50–100 km north of Pataz. Witt *et al.* (2013a) also reported Mesoproterozoic xenocrysts from an andesite dyke that intrudes the batholith near the Glorita mine, in the Pataz district (Figure 2). Therefore, the San Ignacio-Sunsas orogenic belt may have been the lower crustal source for the high-SiO₂ batholith suite, or alternatively a contaminant of melts derived from a source equivalent to the Vijus and Atahualpa formations.

The heat required for melting of the lower crustal source was likely provided by emplacement of fractionated mantle-derived magmas similar in composition to those represented by the low-SiO₂ batholith suite (Figure 15b). Mississippian magmatism commenced with the eruption of the low-SiO₂ batholith magma as the Vista Florida Group volcanic rocks, and emplacement of diorite, microdiorite and diorite porphyry into tensional fractures in the upper crust below the volcanic vents (Witt *et al.* 2013a). Enrichment of Cs and Rb, and positive Pb anomalies in the most primitive samples (WWG24 and WWG28) suggest the low-SiO₂ suite was derived by partial melting of metasomatized mantle, similar to that which yielded the parent magmas for the

Vijus and Atahualpa formations, but with no negative Ti anomaly. This suggests that, whereas the mantle source for the Vijus and Atahualpa formation magmas was depleted by previous melt extraction, the source for the low-SiO₂ Pataz batholith suite was not, requiring regeneration of asthenospheric mantle to replace the depleted source with an undepleted source (Figure 15b). This could occur where upwelling of undepleted asthenosphere was initiated by incipient rifting, although any such rifts did not develop fully into back-arcs. Progressive incorporation of Mesoproterozoic lower crustal material to metasomatized but undepleted asthenospheric melt produced the more evolved samples of the low-SiO₂ suite and led to diminution of the Pb anomaly, but addition of Th, U, K, LREE, MREE and Zr. At some point, a change in the local stress field caused ponding of the low-SiO₂ magma in the lower crust, where partial melting occurred to produce the high-SiO₂ magma.

Within a few million years of the emplacement of the Pataz batholith, renewed crustal melting produced K-rich felsic magmas with A-type affinities, which were erupted as the Lavasen Volcanics and emplaced in a shallow crustal setting as latitic rocks of the Esperanza subvolcanic complex (Figure 15c). In comparison with the

andesitic source for the high-SiO₂ batholith suite, the crustal source for the felsic Esperanza–Lavasen suite was relatively SiO₂- and K-rich (cf. Roberts & Clemens 1993). The residual source is unlikely to be more SiO₂- and K₂O-rich following extraction of the Pataz batholith I-type granodiorite. The San Ignacio–Sunsas orogen embraces a sufficient compositional range to be an appropriate source for the felsic Esperanza–Lavasen suite, consistent with the presence of Mesoproterozoic zircon xenocrysts in the Esperanza subvolcanic complex (Witt *et al.* 2013a). Surface exposures of the compositionally diverse Mesoproterozoic orogen include peraluminous, calc-alkaline to alkali-calcic granitoids with negative Nb–Ta anomalies (Miskovic & Schaltegger 2009; Miskovic *et al.* 2009). However, Mesoproterozoic zircons are rare in the Esperanza–Lavasen felsic suite, as might be expected of alkali-rich magmas. Furthermore, unpublished Lu–Hf isotope data for zircon from a Lavasen sample require a much younger crustal source than the San Ignacio–Sunsas orogen (T. Kemp & T. Angerer, pers. comm., 2011). An alternative source for the Esperanza–Lavasen magmas could be provided by tonalite and granodiorite equivalent to those forming the high-SiO₂ Pataz batholith suite, if some of this magma ponded in the mid crust. This alternative model is consistent with alkali enrichment, positive Pb and negative Nb anomalies on spidergrams for the Esperanza–Lavasen felsic suite. Relatively deep Eu, Sr and P anomalies suggest residual plagioclase and apatite.

It is proposed that the heat required for crustal anatexis of the Esperanza–Lavasen felsic suite source was provided by emplacement of mantle-derived mafic magma. The true nature of this mantle-derived melt is not known, but the relatively mafic compositions of samples 195022 and 195026 provide some evidence for a more mafic component in the A-type magma chamber. The source of the magma was probably similar to that (enriched asthenosphere that had not previously melted), which yielded the low-SiO₂ suite of the batholith. The strong Cs and Rb anomaly, and positive Pb anomaly of the post-lattitic Fe-rich dolerite provide some evidence that this asthenospheric source was melting at the time of A-type magmatism.

A-type granites are generally found in anorogenic settings in continental interiors, but also form at plate margins in the waning stages of subduction zone magmatism where they typically occur on the landward side of subduction-related magmas (Anderson 1983; Eby 1990; Dall’Agnol & de Oliveira 2007), as do the Esperanza subvolcanic complex and the genetically related Lavasen Volcanics. Miskovic *et al.* (2009) reported several intrusions with A-type affinities in the Pataz–Parcoy area of the Eastern Andean Cordillera, ranging in age from Mississippian (333.2 Ma) through to the Middle Jurassic (172.9 Ma). If the SHRIMP U–Pb in zircon age of the Estrella monzonite porphyry can be accepted as a crystallisation age, the age range is extended into the mid Ordovician (Witt *et al.* 2013a). More regionally, these anorogenic and alkaline granites cluster in the Neoproterozoic, Permian–Triassic and Early Jurassic periods (Miskovic *et al.* 2009). The ages determined for the Esperanza–Lavasen felsic suite (*ca* 334 Ma) is mid-Mississippian, and the same age as a monzogabbro from

central Pataz dated by Miskovic *et al.* (2009) as 333.2 ± 7.7 Ma. Miskovic & Schaltegger (2009) interpreted these alkali-rich potassic granites as resulting from crustal underplating by juvenile, mantle-derived magmas during periods of extension. This model is essentially consistent with our proposed model for the Esperanza–Lavasen suite. The close temporal association of the calc-alkaline Pataz batholith and the K-rich Esperanza–Lavasen suite is not unique in arc environments. In northern Luzon, Philippines, overlapping calc-alkaline and alkali-rich magmatism takes place during a transitional period, from the former to the latter (Hollings *et al.* 2011).

The Carboniferous magmatic history of the Pataz district suggests rapidly alternating periods of extension allowing magma to reach the surface and erupt as volcanoes, and compression that impeded the upward movement of mantle-derived magmas and promoted ponding and partial melting in the lower crust (Table 3). Alternations between compression and extension on time-scales of less than a million years are not unusual in the Andes (Mercier *et al.* 1992; James & Sacks 1999). Changes between normal and flat subduction have been proposed to account for similar alternations, but ‘normal–flat–normal’ cycles take *ca* 50 Ma (James & Sacks 1999; Kay *et al.* 1999). Thermal weakening of the crust, during a period of normal subduction and under a consistent external stress field, is proffered as a more viable explanation for rapid switching between extension and compression at Pataz (cf. James & Sacks 1999). During periods of extension and high heat flow that are typically associated with normal subduction, mafic magmas were generated in the mantle wedge and were erupted or emplaced into the upper crust. During these periods, incipient rifting of the arc may have occurred, providing a source for mantle-derived magmas without Nb or Ti anomalies. Over time, the passage of mantle-derived magma weakened the crust, and compressional deformation under the prevailing external stress field obstructed the upward passage of mafic magma, which was then ponded in the lower crust causing partial melting and generation of the more silicic magmas. When sufficient strain had accumulated to again strengthen the crust, extension was re-established, and another phase of magma emplacement or eruption in the upper crust would follow. Additionally, especially in the near surface environment, rapid switching between compressive and extensional tectonics could also be attributed to the transtensional setting of the Pataz–Parcoy gold field in a jog on the regional Cordillera Blanca Fault (Witt *et al.* 2013a).

Implications for gold mineralisation at Pataz

The auriferous quartz veins hosted by the Pataz batholith were emplaced during regional ENE–WSW shortening (Haerberlin *et al.* 2004). Crustal shortening prevented escape of the hydrothermal fluid through subvertical NNW-striking faults and promoted fracture and vertical extension under high fluid pressure, forming mineralised veins preferentially in the rheologically strong Pataz batholith (Witt *et al.* 2013a).

Previous workers have discounted the Pataz batholith as a source for the ore fluid at Pataz on the grounds of

Table 3 Alternating periods of extension and compression during the Mississippian, Pataz district.

| Relative age | Event | Tectonic setting |
|---|--|------------------|
| (Earliest) | | |
| pre- and overlapping 338 to 336 Ma | Eruption of Vista Florida Group and emplacement of low-SiO ₂ batholith suite magma in the mid- to upper crust | Extension |
| 338 to 336 Ma ^{a,b} | Ponding of low-SiO ₂ batholith magma in lower crust and generation of high-SiO ₂ batholith magma | Compression |
| 338 to 336 Ma ^{a,b} | Emplacement of high-SiO ₂ batholith magma into the mid- to upper crust | Extension |
| ca 334 Ma ^b | Ponding of mantle-derived magma in lower crust and generation of the Lavasen-Esperanza suite magma | Compression |
| ca 334 Ma ^b | Formation of Lavasen graben and eruption of Lavasen Volcanics | Extension |
| (Latest) | | |
| ca 332 Ma ^c or 314–312 Ma ^d | Fracture of Pataz batholith and formation of gold-bearing veins | Compression |

^aSchaltegger *et al.* (2006).^bWitt *et al.* (2013a).^cSzappanosné-Vágó *et al.* (2010).^dHaeberlin *et al.* (2004).

incompatibility of age data. However, these age constraints are based largely on Ar–Ar geochronology, which is prone to resetting by later thermal events (Kent & Hagemann 1996; Witt *et al.* 1996; Vielreicher *et al.* 2010). Haeberlin *et al.* (2004) published ⁴⁰Ar/³⁹Ar data from metasomatic white mica alteration halos around mineralised batholith-hosted veins. These data generated plateau at 314–312 Ma, which the authors interpreted as indicative of the age of gold mineralisation, although the ⁴⁰Ar/³⁹Ar data could as well be interpreted as the minimum age for mineralisation.

A recently published Re–Os date for molybdenite from a quartz–arsenopyrite–molybdenite vein in the Parcoy district (Szappanosné-Vágó *et al.* 2010) provides an alternative age for gold mineralisation. Arsenopyrite is abundant in the batholith-hosted auriferous lodes and trace amounts of molybdenite were identified in veins from the northern Pataz district by qualitative SEM analysis (Witt, unpublished data) but this molybdenite has not been dated. The Re–Os age of 331.9 ± 1.7 Ma for molybdenite from Parcoy is within error of the emplacement ages of both the Pataz batholith and the Esperanza subvolcanic complex but is closer to the mean age of the latter (334 Ma; Witt *et al.* 2013a). The batholith-hosted veins post-date high-temperature ductile deformation of batholith contacts (Witt *et al.* 2013a) and formed during subsequent uplift of the batholith (Haeberlin *et al.* 2004). Differential uplift of the Pataz batholith and its country rocks produced the Lavasen graben into which the Lavasen volcanic rocks accumulated, having been erupted from centres such as the Esperanza subvolcanic complex, at the margins of the rift. The age of the Esperanza subvolcanic complex (333.6 ± 2.9 Ma; Witt *et al.* 2013a) is therefore considered close to the age of the batholith-hosted veins. The temporary switch from extension during the main Esperanza–Lavasén magmatic event to shortening during formation of the batholith-hosted veins may be attributed to the ongoing tectonic evolution of the Pataz–Parcoy transtensional jog.

It is further argued that, unlike porphyry deposits, the Pataz batholith does not display evidence of widespread hydrothermal activity (other than propylitic alteration) beyond the proximal illitic alteration zones

surrounding the mineralised veins (Witt *et al.* 2013b). Furthermore, data presented here show that, unlike granites associated with intrusion-related gold deposits (Hart *et al.* 2004; Duuring *et al.* 2007), the Pataz batholith is not highly fractionated.

Not only is the interpreted timing of gold mineralisation broadly constrained as coeval with Esperanza–Lavasén magmatism, but field and petrographic observations suggest widespread hydrothermal activity, contemporaneous with and spatially related to the Esperanza–Lavasén magmatism, summarised as follows. Latitic rocks of the Esperanza subvolcanic complex display evidence for weak but widespread potassic alteration, secondary hematite and argillic alteration. The Fe-rich dolerites of the complex locally display calc-silicate alteration and minor disseminated pyrite and chalcopyrite. Furthermore, textural heterogeneity and the progressive enrichment of Ca in plagioclase suggest increasing water pressure during crystallisation of the dolerite magma (Witt *et al.* 2013a). The presence of late-stage plagioclase–magnetite veinlets in some dolerite samples provides evidence for the generation of a residual, Fe-rich, saline, hydrothermal fluid. This Fe-rich hydrothermal fluid may have contributed to the hydrothermal system that deposited gold-rich quartz veins, locally containing abundant iron and base metal (Pb, Zn) sulfides, in the Pataz batholith. The proposed genetic association between gold mineralisation and a vertically zoned magma chamber containing Esperanza–Lavasén suite magmas is consistent with the worldwide association between gold and K-rich igneous rocks derived from enriched (metasomatised) mantle sources (Muller & Groves 1995), a concept further developed by Hronsky *et al.* (2012). Mafic alkaline magmas in the Bingham and Tintic (Cu–Au–Mo, Ag–Pb–Zn) mining districts, Utah, provide an analogous model to that proposed above for an Fe-rich hydrothermal fluid derived from the mantle-derived component of the Esperanza–Lavasén magma chamber. Keith *et al.* (1997) and Maughan *et al.* (2002) found that mafic alkaline dykes in these mining districts mixed and fractionated at shallow crustal levels to form ore-related latites and monzonites. They also proposed that resorption and oxidation of the abundant sulfide

globules in the mafic magmas may have contributed metals to the ore fluid in these districts.

The Bingham porphyry deposit is a different style of deposit to the metre-scale, batholiths-hosted veins at Pataz, but common processes may give rise to gold deposits encompassing a range deposit classifications (e.g. Hronsky *et al.* 2012). In fact, the overall form of NMORB-normalised spidergrams is very similar to that of mantle-normalised spidergrams for felsic magmas associated with gold mineralisation reported by Hronsky *et al.* (2012). However, analogues of the Pataz batholiths-hosted vein deposits are not commonly described in the geological literature. Orogenic veins, by definition (Groves *et al.* 1998), do not contain the high sulfide content of high-grade shoots at Pataz (Witt *et al.* 2011). The association of gold with Pb and Zn is not typical of porphyry or intrusion-related gold systems where gold tends to be concentrated with Cu in proximal settings and Pb–Zn–Ag concentrated in distal settings (Hart 2005; Sillitoe 2010). Perhaps the closest analogy for Pataz is the Charters Towers district (including Ravenswood) Queensland, Australia, where granitoid-hosted veins, locally containing 90% sulfides (pyrite, galena, sphalerite), are mined for gold (Kreuzer 2005). Like Pataz, the classification of these deposits remains controversial (e.g. Peters 1993; Kreuzer 2005; Bertelli *et al.* 2009).

SUMMARY AND CONCLUSIONS

A curious and distinctive feature of the Pataz igneous rocks is the persistence through time, extending at least from the Ordovician to the late Mississippian, with bulk compositions displaying positive Pb anomalies and enrichment of Cs and Rb. These persistent features suggest the presence of a metasomatised mantle source beneath the Eastern Andean Cordillera since at least Ordovician times. The earliest magmas derived from this mantle source, the Ordovician Vijus and Atahualpa formations, also display a negative Nb anomaly typical of subduction zone magmas and are interpreted to have been derived by partial melting of a depleted mantle source followed by fractional crystallisation and assimilation of continental crust (Figure 15a). The absence of a negative Nb or Ti anomaly in later (Mississippian) mantle-derived magmas requires convection of the asthenosphere or replacement of the depleted mantle source by undepleted asthenosphere (not previously depleted by extraction of a partial melt; Figure 15b, c). The strongest Pb anomalies are found in least evolved magmas of the low-SiO₂ suite of the Mississippian Pataz batholith. Assimilation of continental crust weakened the Pb anomalies in more evolved samples of the suite but added LREE, MREE, Th, U, Zr and P while simultaneously depleting HREE and Y.

Ponding of mantle-derived magmas is proposed as the heat source for melting of the lower to mid continental crust to produce the more felsic Mississippian magmas that constitute the bulk of the Pataz batholith and the slightly later Esperanza–Lavasen suite. These magmas show similar but stronger enrichment of LREE, MREE, Th, U, Zr and P than the contaminated low-SiO₂ suite magmas, and are interpreted to have formed by partial

melting of calc-alkaline dioritic to andesitic lower crust in the case of the Pataz batholith, and of tonalitic middle crust in the case of the Esperanza–Lavasen A-type magmas. Negative Ti anomalies (and Nb anomalies in the case of the Esperanza–Lavasen association) in these magmas were inherited from earlier subduction-related lower to mid crustal source rocks. This model for formation of the high-SiO₂ batholith suite is consistent with the Pb and Nd isotope data of Macfarlane *et al.* (1999), which they interpret to indicate 35 to 70% crustal addition (assimilation of Marañon Complex basement) to a mantle-derived melt. In contrast, our model for the origin of the Mississippian felsic rocks envisages melting of crustal sources with a variable but subordinate to minor contribution from the mantle-derived melt that also provided a heat source.

Mesoproterozoic rocks of the San Ignacio–Sunsas orogen, locally exposed in the central section of the Eastern Andean Cordillera (Miskovic *et al.* 2009), provide a suitable range of compositions for the generation of the high-SiO₂ suite magmas of the Pataz batholith and the Esperanza–Lavasen felsic suite. However, preliminary unpublished Lu–Hf isotope data for zircon from the Esperanza–Lavasen suite (T. Kemp and T. Angerer, pers. comm. 2011) require rapid remelting of mantle-derived source rocks. This could be achieved by melting of mid-crustal tonalite and granodiorite formed by fractionation of magma equivalent to low-SiO₂ suite of the Pataz batholith, if some of that magma ponded in the mid crust. Similarly, the Pataz high-SiO₂ suite may have formed by remelting of lower crustal rocks equivalent to the Vijus and Atahualpa andesites, although Lu–Hf data are not available to support this model.

Although geochronological estimates for the emplacement of the Pataz batholith and the Esperanza–Lavasen suite both overlap with the Re–Os age of molybdenite in a mineralised vein from the Parcoy gold field, geological considerations indicate that the Pataz batholith was slightly earlier, and that the latitic to rhyolitic Esperanza–Lavasen suite magmas provide a viable source for the gold ore fluid. It is suggested that K-rich A-type magma chambers (unexposed but inferred as the source of Lavasen Volcanics and small A-type intrusions) belonging to this suite may be genetically related to gold in the Pataz district, but also more widely in the Eastern Andean Cordillera, consistent with the worldwide association between gold and K-rich igneous rocks (Muller & Groves 1995).

ACKNOWLEDGEMENTS

The content of this paper benefited from conversations and e-mail exchange between the authors and Diego Sologuren, Alex Miskovic, Thomas Angerer and Tony Kemp. Constructive advice and reviews of the manuscript prior to submission were provided by Kevin Cassidy, Roger Bateman, Paul Durning and Tony Kemp. Col Steele assisted with drafting of some of the figures. The paper is published with permission of Compania Minera Poderosa S.A., who funded the study reported here and provided logistic support in the field. The authors also acknowledge constructive reviews by David Champion and an anonymous journal reviewer.

REFERENCES

- ANDERSON J. L. 1983. Proterozoic anorogenic granite plutonism of North America. *Geological Society of America Memoir* **161**, 133–154.
- BAHLBERG H. & HERVE F. 1997. Geodynamic evolution and tectonostratigraphic terranes of northwestern Argentina and northern Chile. *Geological Society of America Bulletin* **109**, 869–884.
- BARNES C. G. 1983. Petrology and upward zonation of the Wooley Creek Batholith, Klamath Mountains, California. *Journal of Petrology* **24**, 495–537.
- BATEMAN P. C. & CHAPPELL B. W. 1979. Crystallization, fractionation and solidification of the Tuolumne intrusive series, Yosemite National Park, California. *Geological Society of America Bulletin* **90**, 463–482.
- BERTELLI M., WILLIAMS P. J., BAKER T., LISOWIEC N. & BOYCE A. 2009. Nature and origin of ore-forming fluids in the Ravenswood gold system, north Queensland: Evidence from fluid inclusions and stable isotopes. In: Williams P. J. et al. eds. Proceedings of 10th Biennial SGA Meeting, Townsville, Australia, 2009, pp. 344–346. *Economic Geology Research Unit, James Cook University, Townsville, Queensland, Australia*.
- BOYNTON W. V. 1984. Cosmochemistry of the rare earth elements: meteoritic studies. In: *Rare earth chemistry*, pp. 63–114. Elsevier, Amsterdam.
- BROWN G. C., THORPE R. S. & WEBB P. C. 1984. The geochemical characteristics of granitoids in contrasting arcs and comments on magma sources. *Journal of the Geological Society of London* **141**, 413–426.
- CHAPPELL B. W. & STEPHENS W. E. 1988. Origin of infracrustal (I-type) granite magmas. *Transactions of the Royal Society of Edinburgh, Earth Sciences* **79**, 71–86.
- CHAPPELL B. W. & WHITE A. J. R. 1974. Two contrasting granite types. *Pacific Geology* **8**, 173–174.
- CHAPPELL B. W. & WHITE A. J. R. 1992. I- and S-type granites of the Lachlan fold belt. *Royal Society of Edinburgh Transactions* **83**, 1–26.
- CHEW D. M., SCHALTEGGER U., KOSLER J., WHITEHOUSE M. J., GUTJAHR M., SPIKINGS R. A. & MISKOVIC A. 2007. U–Pb geochronologic evidence for the evolution of the Gondwana margin of the north-central Andes. *Geological Society of America Bulletin* **119**, 687–711.
- COCHERIE A. 1986. Systematic use of trace element distribution patterns in log–log diagrams for plutonic suites. *Geochimica et Cosmochimica Acta* **50**, 2517–2522.
- COLLINS W. J., BEAMS S. D., WHITE A. J. R. & CHAPPELL B. W. 1982. Nature and origin of A-type granites with particular reference to southeastern Australia. *Contributions to Mineralogy and Petrology* **80**, 189–200.
- COX K. G., BELL J. D. & PANKHURST R. J. 1980. *The interpretation of igneous rocks*. George Allen and Unwin, London, 450 pp.
- CREASER R. A. 1996. Petrogenesis of a Mesoproterozoic quartz latite-granitoid suite from the Roxby Downs area, South Australia. *Precambrian Research* **70**, 371–394.
- CREASER R. A., PRICE R. C. & WORMALD R. J. 1991. A-type granites revisited: Assessment of a residual-source model. *Geology* **19**, 163–166.
- DALL'AGNOL R. & DE OLIVEIRA D. C. 2007. Oxidized, magnetite-series, rapakivi-type granites of Carajas, Brazil: Implications for classification and petrogenesis of A-type granites. *Lithos* **93**, 215–233.
- DUURING P., CASSIDY K. F. & HAGEMANN S. G. 2007. Granitoid-associated orogenic, intrusion-related, and porphyry style metal deposits in the Archean Yilgarn Craton, Western Australia. *Ore Geology Reviews* **32**, 157–186.
- EBY G. N. 1990. The A-type granitoids: A review of their occurrence and chemical characteristics and speculations on their petrogenesis. *Lithos* **26**, 115–134.
- ELLIOTT T., PLANK T., ZINDLER A., WHITE W. & BOURDON B. 1997. Element transport from slab to volcanic front at the Mariana arc. *Journal of Geophysical Research* **102**, 14991–15019.
- FROST C. D. & FROST B. R. 1997. Reduced rapakivi type granites: the tholeiite connection. *Geology* **25**, 647–650.
- FROST R. B., BARNES C. G., COLLINS W. J., ARCULUS R. J., ELLIS D. J. & FROST C. D. 2001. A geochemical classification for granitic rocks. *Journal of Petrology* **42**, 2033–2048.
- GROVES D. I., GOLDFARB R. J., GEBRE-MIRIAM M., HAGEMANN S. G. & ROBERT F. 1998. Orogenic gold deposits: A proposed classification in the context of their crustal distribution and relationship to other gold deposit types. *Ore Geology Reviews* **13**, 7–27.
- HALE A. J., GOTTSCHALDT K.-D., ROSENBAUM G., BOURGOUIN L., BAUCHY M. & MÜHLHAUS H. 2009. Dynamics of slab tear faults: insights from numerical modeling. *Tectonophysics* **483**, 58–70.
- HART C. J. R. 2005. Classifying, distinguishing and exploring for intrusion-related gold systems. *The Gangue MDD Newsletter* **87**, 4–9.
- HAEBERLIN Y., MORITZ R., FONTBOTE L. & COSCA M. 2004. Carboniferous orogenic gold deposits at Pataz, Eastern Andean Cordillera, Peru: geological and structural framework, paragenesis, alteration, and $^{40}\text{Ar}/^{39}\text{Ar}$ geochronology. *Economic Geology* **99**, 73–112.
- HART C. J. R., MAIR J. L., GOLDFARB R. J. & GROVES D. I. 2004. Source and redox controls on metallogenic variations in intrusion-related ore systems, Tombstone-Tungsten Belt, Yukon Territory, Canada. *Transactions of the Royal Society of Edinburgh, Earth Sciences* **95**, 339–356.
- HRONSKY J., GROVES D. I., LOUCKS R. R. & BEGG G. C. 2012. A unified model for gold mineralisation in accretionary orogens and implications for regional-scale exploration targeting method. *Mineralium Deposita* **47**, 339–358.
- HOLLINGS P., WOLFE R., COOKE D. R. & WATERS P. J. 2011. Geochemistry of Tertiary igneous rocks of northern Luzon, Philippines: evidence for a back-arc setting for alkalic porphyry copper–gold deposits and a case for slab roll-back? *Economic Geology* **106**, 1257–1278.
- HYNDMAN D. W. 1984. A petrographic and chemical section through the northern Idaho batholith. *Journal of Geology* **92**, 83–102.
- JAMES D. E. & SACKS I. S. 1999. Cenozoic formation of the Central Andes: a geophysical perspective. In: Skinner B. J. ed. *Geology and ore deposits of the Central Andes*, pp. 1–25. Society of Economic Geologists Special Publication 7.
- JAQUES A. L. & GREEN D. H. 1980. Anhydrous melting of peridotite at 0–15 kb pressure and the genesis of tholeiitic basalts. *Contributions to Mineralogy and Petrology* **73**, 287–310.
- JENNER G. A. 1996. Trace element geochemistry of igneous rocks: Geological nomenclature and analytical geochemistry. In: Wyman D. A. ed. *Trace element geochemistry of volcanic rocks*, pp. 51–78. Geological Association of Canada Short Course Notes 12.
- KAY S. M., MPODOZIS C. & COIRA B. 1999. Neogene magmatism, tectonism and mineral deposits of the central Andes (22° to 33° S Latitude). In: Skinner B. J. ed. *Geology and ore deposits of the Central Andes*, pp. 27–59. Society of Economic Geologists Special Publication 7.
- KEITH J. D., WHITNEY J. A., HATTORI K., BALLANTYNE G. H., CHRISTIANSEN E. H., BARR D. L., CANNAN T. M. & HOOK C. J. 1997. The role of magmatic sulphides and mafic alkaline magmas in the Bingham and Tintic mining districts, Utah. *Journal of Petrology* **38**, 1697–1690.
- KENT A. J. R. & HAGEMANN S. G. 1996. Constraints on the timing of lode gold mineralization in the Wiluna greenstone belt, Yilgarn craton, Western Australia. *Australian Journal of Earth Sciences* **43**, 573–588.
- KREUZER O. P. 2005. Intrusion-hosted mineralization in the Charters Towers Goldfield, north Queensland: new isotopic and fluid inclusion constraints on the timing and origin of the auriferous veins. *Economic Geology* **100**, 1583–1603.
- MACFARLANE A. W., TOSDAL R. M., VIDAL C. & PAREDES J. 1999. Geologic and isotopic constraints on the age and origin of auriferous quartz veins in the Parcoy mining district, Pataz, Peru. In: Skinner B. J. ed. *Geology and ore deposits of the Central Andes*, pp. 267–279. Economic Geology Special Publication 7.
- MAUGHAN D. T., KEITH J. D., CHRISTIANSEN E. H., PULSHIPER T., HATTORI K. & EVANS N. J. 2002. Contributions from mafic alkaline magmas to the Bingham porphyry Cu–Au–Mo deposit, Utah, USA. *Mineralium Deposita* **37**, 14–37.
- McCULLOCH M. T. & GAMBLE J. A. 1991. Geochemical and geodynamical constraints on subduction zone magmatism. *Earth and Planetary Science Letters* **102**, 358–374.
- MEGARD F. 1984. The Andean orogenic period and its major structures in central and northern Peru. *Journal of the Geological Society of London* **141**, 893–900.
- MERCIER J. L., SEBRIER M., LAVENU A., CABRERA J., BELLIER O., DUMONT J.-F. & MACHARE J. 1992. Changes in the tectonic regime above a subduction zone of Andean type: the Andes of Peru and Bolivia during the Pliocene–Pleistocene. *Journal of Geophysical Research* **97**, 11945–11982.
- MISKOVIC A. & SCHALTEGGER U. 2009. Crustal growth along a non-collisional cratonic margin: A Lu–Hf isotopic survey of the

- Eastern Cordillera granitoids of Peru. *Earth and Planetary Science Letters* **279**, 303–315.
- MISKOVIC A., SCHALTEGGER U. & CHEW D. 2006. Carboniferous plutonism along the Eastern Peruvian Cordillera: implications for the late Paleozoic to Early Mesozoic Gondwana tectonics. XIII Congreso Peruano de Geología, Lima, 17–20 October 2006 (Abstract).
- MISKOVIC A., SPIKINGS R. A., CHEW D. M., KOALER J., ULIANOV A. & SCHALTEGGER U. 2009. Tectonomagmatic evolution of Western Amazonia: Geochemical characterization and zircon U–Pb geochronologic constraints from the Peruvian Eastern Cordilleran granitoids. *Geological Society of America Bulletin* **121**, 1298–1324.
- MULLER D. & GROVES D. I. 1995. *Potassic igneous rocks and associated gold–copper mineralization*. Springer, New York, 238 pp.
- NOBLE D. C. & MCKEE E. H. 1999. The Miocene metallogenic belt of central and northern Peru. In: Skinner B. J. ed. *Geology and ore deposits of the Central Andes*, pp. 155–193. Society of Economic Geologists Special Publication 7.
- PANJASAWONG Y., DANYUSHEVSKY L. V., CRAWFORD A. J. & HARRIS K. L. 1995. An experimental study of the effects of melt composition on plagioclase melt equilibria at 5 and 10 kbar: implications for the origin of magmatic An plagioclase. *Contributions to Mineralogy and Petrology* **118**, 420–432.
- PEARCE J. A. 1982. Trace element characteristics of lavas from destructive plate boundaries. In: Thorpe R. S. ed. *Andesites: orogenic andesites and related rocks*, pp. 523–548. John Wiley, Chichester, UK.
- PEARCE J. A. 1983. Role of sub-continental lithosphere in magma genesis at active continental margins. In: Hawkesworth C. J. & Norry M. J. eds. *Continental basalts and mantle xenoliths*, pp. 230–249. Shiva Publishing, Nantwich, UK.
- PEARCE J. A. 1996. A user's guide to basalt discrimination diagrams. In: Wyman D. A. ed. *Trace element geochemistry of volcanic rocks*, pp. 79–114. Geological Association of Canada Short Course Notes 12.
- PEARCE J. A., HARRIS N. B. W. & TINDLE A. G. 1984. Trace element discrimination diagrams for the tectonic interpretation of granitic rocks. *Journal of Petrology* **25**, 956–983.
- PECERILLO A. & TAYLOR S. R. 1979. Geochemistry of Eocene calc-alkaline volcanic rocks from the Kastamonu area, northern Turkey. *Contributions to Mineralogy and Petrology* **58**, 63–81.
- PETERS S. G. 1993. Formation of ore shoots in mesothermal gold–quartz vein deposits: examples from Queensland, Australia. *Ore Geology Reviews* **8**, 277–301.
- PETERSEN U. 1999. Magmatic and metallogenic evolution of the central Andes. In: Skinner B. J. ed. *Geology and ore deposits of the Central Andes*, pp. 109–153. Society of Economic Geologists, Special Publication 7.
- PETFORD N. & ATHERTON M. P. 1992. Granitoid emplacement and deformation along a major crustal lineament. The Cordillera Blanca, Peru. *Tectonophysics* **205**, 171–185.
- PITCHER W. S. 1997. *The Nature and Origin of Granite*. Springer, 387pp.
- PRICE R. C., STEWART R. B., WOODHEAD J. D. & SMITH I. E. M. 1999. Petrogenesis of high-K arc magmas: evidence from Egmont Volcano, North Island, New Zealand. *Journal of Petrology* **40**, 167–197.
- REYES L. & WILSON J. 1964. Geología del Cuadrángulo de Pataz: *INGEMETT (Geological Survey of Peru), National Geological Map, A Series*, 91 pp.
- ROBERTS M. P. & CLEMENS J. D. 1993. Origin of high-potassium, calc-alkaline, I-type granitoids. *Geology* **21**, 825–828.
- SCHALTEGGER U., CHEW D. & MISKOVIC A. 2006. Neoproterozoic to early Mesozoic evolution of the western Gondwana margin: evidence from the Eastern Cordillera of Peru. XIII Congreso Peruano de Geología, Lima, Octubre 2006 (extended abstract).
- SCHREIBER D. W., FONTBOTE L. & LOCHMANN D. 1990. Geologic setting, paragenesis, and physicochemistry of gold quartz veins hosted by plutonic rocks in the Pataz region. *Economic Geology* **85**, 1328–1347.
- SHAND S. J. 1943. *Eruptive rocks: their genesis, composition, classification and their relation to ore deposits*. John Wiley and Sons, London, UK.
- SILLITOE R. H. 2010. Porphyry copper systems. *Economic Geology* **105**, 3–41.
- SPARKS R. S. J., HUPPERT H. E., TURNER J. S., SAKUYAMA M. & O'HARA M. J. 1984. The fluid dynamics of evolving magma chambers. *Philosophical Transactions of the Royal Society A* **310**, 511–534.
- SUN S. S. & McDONOUGH W. F. 1989. Chemical and isotope systematic of oceanic basalt: implications for mantle composition and process. In: Sanders A. D. & Norrish M. J. eds. *Magmatism in the ocean basins*, pp. 313–346. Blackwell Science, Cambridge, MA.
- SZAPPANOSNE-VAGÓ E., MORITZ R. & BARRA F. 2010. Fluid inclusion investigation and Re–Os dating of the Pataz–Parcoy intrusion-hosted gold deposits, Eastern Cordillera, Peru. International Mineralogical Association, IMA2010 Conference Abstracts, Budapest, Hungary, p. 260.
- TURNER S. P., FODEN J. D. & MORRISON R. S. 1992. Derivation of some A-type magmas by fractionation of basaltic magma: An example from the Padthaway ridge, South Australia. *Lithos* **28**, 151–179.
- VIELREICHER N. M., GROVES D. I., SNEE L. W., FLETCHER I. R. & MCNAUGHTON N. J. 2010. Broad synchronicity of three gold mineralization styles in the Kalgoorlie gold field: SHRIMP, U–Pb, and ⁴⁰Ar/³⁹Ar geochronological evidence. *Economic Geology* **105**, 187–228.
- WHALEN J. B., CURRIE K. L. & CHAPPELL B. W. 1987. A-type granites: geochemical characteristics, discrimination and petrogenesis. *Contributions to Mineralogy and Petrology* **95**, 407–419.
- WILSON M. 1989. *Igneous petrogenesis: A global tectonic approach*. Harper Collins, London, 466 pp.
- WILSON J. J. & REYES L. 1997. Mapa Geológico Cuadrángulo del Pataz. *INGEMMET 1:100 000 geology series map*, Quadrangle 16b.
- WINCHESTER J. A. & FLOYD P. A. 1977. Geochemical discrimination of different magma series and their differentiation products using immobile elements. *Chemical Geology* **20**, 325–343.
- WITT W. K., HAGEMANN S. G., OJALA J., LAUKAMP C., VENNEMANN T., VILLANES C. & NYKANEN V. 2013b. Multiple methods for regional- to mine-scale targeting, Pataz gold field, northern Peru. *Australian Journal of Earth Sciences*, <http://dx.doi.org/10.1080/08120099.2013.763859>.
- WITT W. K., HAGEMANN S. G., VILLANES C. & QINGTAO ZENG 2013a. New geochronological results and structural evolution of the Pataz gold mining district: implications for the timing and origin of the batholith-hosted veins. *Ore Geology Reviews* **50**, 143–170.
- WITT W. K., HAGEMANN S. G., VILLANES C., SOLOGUREN D., VENNEMANN T., ZWINGMANN H. & JOURDAN F. 2011. A >3 km vertical section through mesothermal to epithermal levels of a Carboniferous, alkali intrusion-related hydrothermal system in the Eastern Andean Cordillera, Pataz, northern Peru. SGA Conference, Antafogasta, Chile 2011, Extended Abstracts Volume.
- WITT W. K., SWAGER C. P. & NESLON D. R. 1996. ⁴⁰Ar/³⁹Ar and U–Pb age constraints on the timing of gold mineralization in the Kalgoorlie gold fields, Western Australia—a discussion. *Economic Geology* **91**, 792–795.

Received 2 July 2012; accepted 12 April 2013

SUPPLEMENTARY PAPERS

Whole-rock analytical methods.

Table A1 Whole-rock geochemical samples, location and description.

Table A2 Results of whole-rock geochemical analyses.